THE APPLICATION OF NUCLEAR PHYSICS PROCESSES FOR DIAMOND DETECTION WITHIN KIMBERLITE

PW MAMPE

Dissertation submitted in partial fulfilment of the requirements for the degree of Master of Science in Applied Radiation Science at the Mafikeng Campus of the North-West University

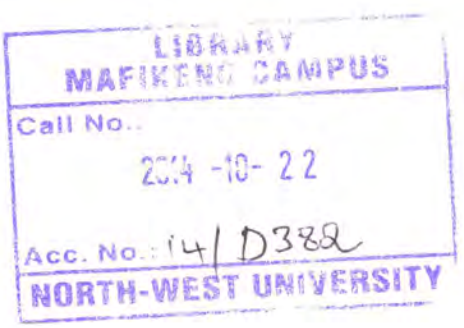

Supervisor: Prof. S.H Connell

Co-supervisor: Mr S Ballestrero

October 2013

Contents

List of Figures

List of Tables

LIST OF ABBREVIATIONS

ADC	Analog to Digital Converter
BaF_2	Barium Fluoride
BGO	Bismuth Germanate
CAMAC	Electronic CAMAC data acquisition system
CFD	Constant Fraction Discriminator
DAQ	Data Acquisition System
G and D	Gate and Delay Generator
GDR	Giant Dipole Resonance
NaI (Tl)	Thallium-activated sodium iodide
PET	Positron Emission Tomography
PMT	Photomultiplier Tube
PS-PMT	Position Sensitive Photomultiplier Tube
Quad	Quadruple Amplifier
RM	Rate Meter
SA	Spectroscopy Amplifier
SCA	Single Channel Analyzer
TAC	Time to Amplitude Converter
TDC	Time to Digital Converter
X_o	Absorption length

Declaration

I hereby declare that

THE APPLICATION OF NUCLEAR PHYSICS PROCESSES FOR DIAMOND DETECTION WITHIN KIMBERLITE"

is my own work and has not been submitted for a degree or other qualification to any other university or institution. It is submitted in fulfilment of the requirements for the degree of Masters of Science at North West University.

Penina Welheminah Mampe

Signature _____

19TH day of SEPTEMBER 2014

Acknowledgements

I would like to thank the following:

- Prof. Connell and Mr Ballestrero for the excellent supervision, fruitful discussions, encouragement and their contribution in organizing the funding of this project.
- North West University, Centre of Applied Radiation Science and Technology (CARST) for giving me this opportunity to further my studies and the great experience gained from this field.
- The Physics Department of the University of the Witwatersrand for giving me opportunity to utilise their libraries facilities.
- The staff of iThemba LABS for granting me the opportunity to conduct research and providing equipment facilities.
- The National Research Foundation (NRF), Pebble Bed Modular Reactor (PBMR), Bateman Mineral and CARST for their financial assistance during the course of this research.
- Mr Madhuka and Mr Phoku for their support, effort and encouragement.
- My father and mother for their love, patience, inspiration and encouragement.

Abstract

Mineral-PET (Positron Emission Tomography) is a new concept envisaged to revolutionize diamond-mining operations. The idea is that diamond inclusions may be detected at an early stage. This allows for rejection of barren material from the processing stream, which greatly reduces the costs. The diamond recovery may also be more efficient. In fact, not only the presence but also the size and relative position of the diamond inclusion in the host kimberlite rock may be determined. This allows for grading and differentiated extraction techniques, which may protect larger diamonds. The process involves the use of the (γ,n) interaction at the Giant Dipole Resonance energy of carbon to produce a radioactive carbon-11 PET isotope to label the presence of possible diamonds. This is followed by the use of an analogue of the medical Positron Emission Tomography (PET) diagnostic method to detect the evidence of diamonds in the kimberlite.

The Mineral-PET process has an activation stage, to generate the ^{11}C positron-emitting isotope in the kimberlite, and a detection stage, where the occurrence of hot-spots in the PET signal may distinguish diamondiferous from barren kimberlite. This dissertation makes a contribution in the detection part. Specifically, experimental work has been done on absorption length measurements for kimberlite, as well as a study of the noise reduction capacity of the co-incident detection technique. The former measurement was used as input for computational simulations. The latter measurement was part of the verification of the feasibility calculation for the system as a whole.

Computer modeling by Monte Carlo methods has been used in order to simulate the Mineral-PET system. In this work, the aspects of the Mineral-PET system that were simulated relate to the efficiency of the detectors and the absorption length of radiation by the kimberlite.

Chapter 1

Introduction

1.1 Mineral Positron Emission Tomography concepts

The extraction of diamonds from excavated rocks is presently a complex process which requires large amounts of equipment, energy and water. The large rocks are initially reduced in size, by means of a crusher with counter-rotating cylinders, to particles of approximately 10 to 15 cm diameter, using water both to cool the system and to contain volatile dust. The rocks are further reduced in size, and subsequently processed by a Dense Media Separator (DMS) system. There could be several such stages. The final crush could be down to a few millimeters. In this way, the entire run of mine is subjected to energy and water intensive process, in particular, the vast majority of barren kimberlite rock is processed to the final stage.

The Mineral Positron Emission Tomography (PET) system is being studied for its feasibility. Mineral-PET is a newly developed rock-sorting technique used to detect a possible diamond inclusion within the kimberlite host in an on-line situation. The Mineral-PET process has an activation stage, to generate the ^{11}C positron-emitting isotope in the kimberlite, and a detection stage, where the occurrence of hot-spots in the PET signal may distinguish a diamondiferous from barren kimberlite. This system could potentially reduce the cost of operations in diamond mining industries. The Mineral-PET system serves to offer a high technology solution for sorting of barren from diamondiferous ore. This would present a more competitive and cost effective diamond sorting technique. Diamond inclusions could be detected at an early stage, and not only their presence but also their size and their relative position in the host kimberlite rock can be identified. The Mineral-PET system has a requirement in respect of the minimal size of one cubic millimeter ($1mm^3$) for the diamond to be recovered [1].

This dissertation makes a contribution in the detection part of Mineral PET system. Specifically, experimental work has been done on absorption length measurement for kimberlite, as well as a study of the noise reduction capacity of the co-incident detection technique. The former measurement was used as inputs for computational simulations discussed later. The latter measurement was part of the verification of the feasibility calculation for the system as a whole.

In the Mineral-PET ore-sorting method, kimberlite rock is firstly passed through a photon irradiation stage and secondly through a detection stage. The irradiation system produces photons at the Giant Dipole Resonance (GDR) energy of carbon (a very broad peak centered at 22.5 MeV). The GDR occurs when a nucleus is excited by a gamma ray which is absorbed. The oscillating electromagnetic field of the gamma ray may be thought of as causing a charge oscillation of the nucleus where the protons and the neutrons move counter to each other while the centre of mass of the nucleus remains stationary. When the nucleus stops oscillating, its excess energy is emitted as either gamma radiation, neutrons or charged particles. The most important decay product for this work is carbon-11 resulting from the channel with the emitted neutron [2].

High energy photons are used to activate the kimberlite, which has been pre-crushed to a coarse size of about 10 cm in diameter. This photon irradiation induces amongst other reactions, a small amount of PET isotopes by the (γ,n) reaction. A PET isotope is suitable for imaging by a PET system. The PET isotope of interest is carbon-11 (^{11}C), which is dominantly concentrated in diamond particles which may be in the kimberlite. The rock stream is then passed through a linear PET array, which detects the presence of diamonds as a partially imaged statistically significant hot spot or PET signal [1].

Computer modeling by Monte Carlo methods has been used in order to simulate the Mineral-PET system. In this method, a numerical estimate of the solutions is obtained by averaging over a very large number of iterated calculations. The large number of iterated calculations is based on a sequence of random variables that are used to sample from the distributions applicable to the problem. In this work, the aspects of the Mineral-PET system that was simulated relate to the efficiency of the detectors and the absorption length of radiation by the kimberlite.

In general, there are several techniques used to identify a possible diamond inclusion within kimberlite. For example, one of the techniques involved is the use of X-ray radiography [3]. A second is neutron radiography [4]. X-rays available from normal laboratory sources are not very pene-

trating, whereas neutrons are very penetrating, and neutron radiography is therefore a potential imaging technique for this application where large rocks are involved.

Neutron radiography is based on the principle that neutrons interact with the nucleus of the atom and that each atomic nucleus has a different probability for absorbing or scattering a neutron. The absorption of X-rays or γ-rays increases as the atomic number of the absorber increases. Neutrons are attenuated by some light materials, such as hydrogen (H), boron (B), and lithium (Li), but penetrate many heavy material such as titanium (Ti) and lead (Pb). Neutron radiography can be used in quality control inspection for micro cracks and deformities in metal alloy castings; the study of radioactive samples; imaging of carbon, gun powder grain structure, plastics, lead, and other heavy metals; the determination of pyrotechnic product quality; and the analysis of O-ring placement.

The X-ray radiography technique is also sometimes used. The disadvantages of using X-ray radiography are due to the minimal density contrast between the diamond and host material, and also to its limitation to smaller kimberlite material particles as X-rays are quickly absorbed. Therefore all the kimberlite rocks have to be processed and crushed to small pieces, requiring large equipment and considerable use of energy, moreover large diamonds may be destroyed in the process.

X-ray flourescence is also often used, but here the diamonds must be exposed or liberated, not locked within the kimberlite, as will be the case for lost diamonds.

There is a new alternative, not yet used in mining but in diagonostic medicine. The detection system for this work is based on the Positron Emission Tomography (PET) imaging method, related to that used in diagnostic medicine. The fingerprint occurrence of a PET isotope is the detection of two photons released in coincidence and back-to-back upon the positron annihilation process. The two opposite points given by the detection of photons create a line (broadened by the position resolution), which is called a tube. The actual source point in the tube of the two coincident and anti-co-linear photons is not known.

Position sensitive detectors with excellent time and position resolution are used to accurately identify the gamma coincidences and to locate the positions of the endpoints of the tube relative to the rock. In Mineral-PET, the actual size of the inclusion and its approximate location are derived from a statistical treatment of the intersections formed by reconstruction of the many tubes representing the correlated two photon trajectories from many decay events. The Mineral-PET method is

therefore not a full imaging algorithm as in medical-PET. It has to operate sufficiently fast for real time processing of rock in a conveyor belt situation. The fast gamma radiation sensitive detectors with excellent time and position resolution are configured in a dual planar array placed on top and below the conveyor belt containing the kimberlite rock.

Figure 1.1 shows a schematic overview of the Mineral-PET system process, where the 22.5 MeV irradiator firstly activates the carbon using the nuclear (γ,n) reaction and secondly the detection system which locates the activated carbon which has undergone transmutation in the photonuclear reaction.

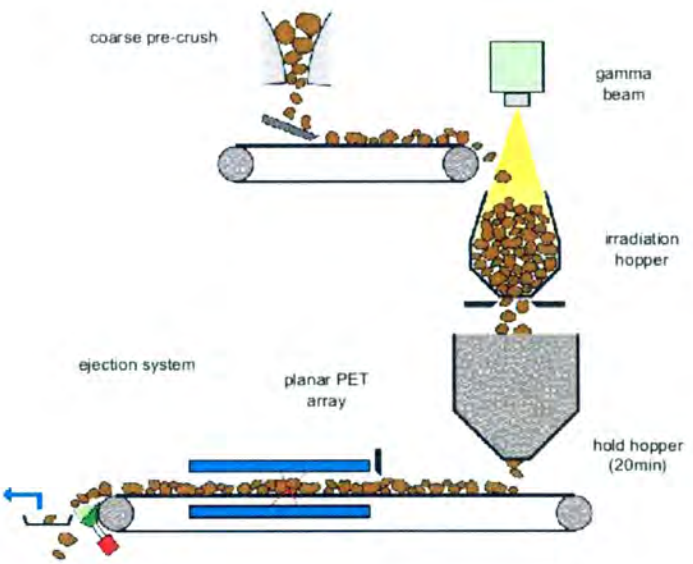

Figure 1.1: An illustration of the Mineral-PET process

1.2 Medical-PET

1.2.1 Introduction

Medical PET is an imaging technique that uses short-lived radioactive substances (radiotracers) to produce three-dimensional images of various components functioning in the body [5]. The radiotracer is injected into the bloodstream, swallowed by mouth or inhaled as a gas. This radiotracer accumulates in the organ or area of the body being examined, where it gives off a small amount of energy in the form of gamma rays. A PET scanner or gamma camera detects this energy and with the help of a computer creates pictures offering details on both the structure and function of organs and other parts of the body.

In particular, a PET scan may be used to detect cancer; determine how much a cancer has spread in the body; determine if a cancer has returned after treatment; assess the effectiveness of a treatment plan such as cancer therapy; determine blood flow to the heart muscle; determine the effects of a heart attack, or myocardial infarction; evaluate brain abnormalities such as tumors, memory disorders and seizures and other central nervous system disorders; and to map normal human brain and heart function [6].

The advantages of PET scanning are provision of detailed diagnostic information not averaged from other imaging tests, earlier detection of disease with fewer invasive diagnostic procedures, better distinction between physiological uptake and pathological uptake, consolidation of patients imaging studies, shorter scanning time, and improved staging of the disease, and better monitoring of cancer reoccurrences [7].

1.2.2 The physical process of the Medical-PET

Before a PET scan is conducted a radioactive substance (such as glucose labeled with a PET isotope) that decays by emitting a positron, is injected into the bloodstream. Such a substance is called a tracer [5]. The positron-emitting isotopes have short half-lives such as carbon-11 (^{11}C) (20 min), nitrogen-13 (^{13}N) (10 min), fluorine-18 (^{18}F) (110 min), and oxygen-15 (^{15}O) (2 min) [8].

The molecule most commonly used is ^{18}F inserted in fluorodeoxyglucose (FDG or 2-fluoro-2-deoxy-D-glucose). FDG can be used for diagnosis, staging and monitoring treatment of cancer. The distribution of a ^{18}F-FDG is a good reflection of the distribution of glucose uptake and phos-

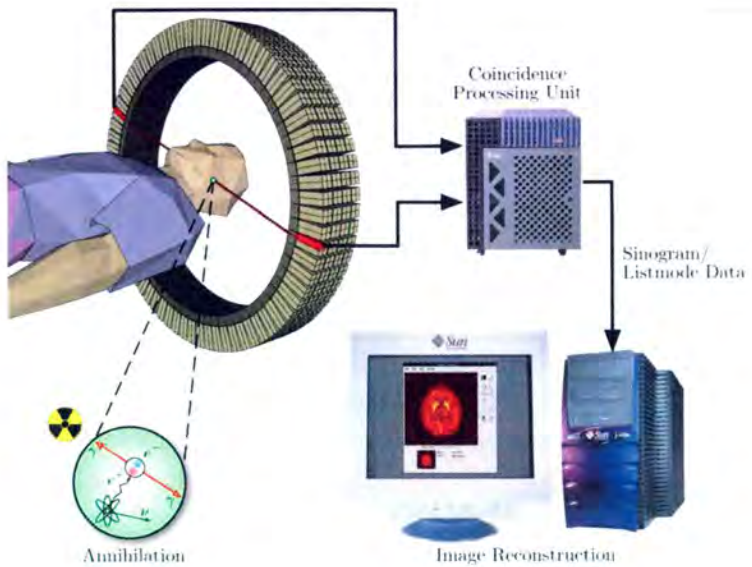

Figure 1.2: Schematic of a Positron Emission Tomography acquisition process [5]

)horylation in the body [9].

Γhere is a waiting period while the active molecule becomes concentrated in the tissue of interest. Γhe patient will be positioned on an examination table that slides into the middle of the scanner Figure 1.2). The active molecule will emit a positron in the process of decay. The positron vill collide with an electron and annihilate with each other to produce two photons of 511 keV ravelling in opposite directions at nearly 180^0 to each other at the same time. These photons are letected when they reach a scintillator material in the scanning device, converting a fraction of the ıbsorbed gamma ray energy into visible photons [10].

Γhe scintillation process consists of a high energy photon (γ ray) incident on the scintillator and :reates an energetic electron, either by Compton scattering or the photoelectric effect. As the :lectron passes through the scintillator, it loses energy and excites other electrons in the process. Γhe scintillating materials decay back to their ground state, emitting visible light. The scintillator s optically coupled to a photomultiplier tube (PMT) which then generates an electrical signal in 'esponse to light incident to its surface. An electrical signal is generated with a width, amplitude, ınd time relation to the absorption of the photon by the detector [11].

Γhe 511 keV γ photons in PET are best detected with inorganic single-crystal scintillation ma-

terials, because of their higher density and higher atomic number, which lead to better detection efficiency. The conversion process typically takes place on a time scale of nanoseconds to microseconds, thus producing a pulse of photons corresponding to each γ-ray that interacts with the scintillation material. The materials mostly used are bismuth germanate ($Bi_4Ge_3O_{12}$) or BGO, barium fluoride (BaF_2), cerium-doped lutetium oxyorthosilicate (Gd_2SiO_5)[Ce] or GSO, cerium-doped gadolinium oxyorthosilicate (Lu_2SiO_5)[Ce] or LSO and thallium-activated sodium iodide (NaI (Tl)) [10].

Table 1.1 shows the physical properties of some important scintillator materials. Both BGO and LSO have excellent physical properties. They have higher densities and higher atomic numbers that result in efficient detection of γ-rays and they are also rugged and nonhygroscopic, which allows relatively simple detector fabrication. GSO is also a good scintillator, except that it cleaves easily, which makes detector fabrication more difficult. BaF_2 has the shortest decay constant, where the emission is weak and located in the far wavelength of 220 nm, which requires PMT's with more expensive quartz windows. LSO has the best combination of a short decay constant (40 ns) and high emission intensity [12].

Table 1.1: Physical Properties of some important scintillators [12]

Scintillator	BGO	LSO	NaI	BaF_2	GSO
Density (g/cm^3)	7.13	7.40	3.67	4.88	6.71
Effective Z	75	65	51	53	59
Decay Constant(ns)	300	40	230	0.8	56
Hygroscopic	No	No	Yes	No	No
Rugged	No	Yes	No	Yes	No
Wavelength(nm)	480	420	410	220	430

The accuracy of the localization of the gamma hit point in PET depends in part on the position resolution of the detector system. The detector material primarily affects the detection efficiency for the annihilation radiation and secondarily affects the shape of the response near the edge of the detector. The physical limit of accuracy of localization in PET depends on the energy of emission of the positron, and it may annihilate some distance away from its point of emission. In addition, not all the annihilation photons are emitted at exactly 180^0 to each other [11].

During the overlap coincidence method, the width of the timing signal is chosen to ensure that most of the signals from true coincidences will fall into the electronic coincidence time window.

Because of the finite width of these timing signals, there is a probability that unrelated photons will accidentally produce timing signals that will overlap and produce accidental or random coincidences. Accidental and scatter coincidences are the two primary sources of background noise in PET (Figure 1.3). In order to establish that annihilation photons are in coincidence in PET system, it is necessary to perform timing measurements.

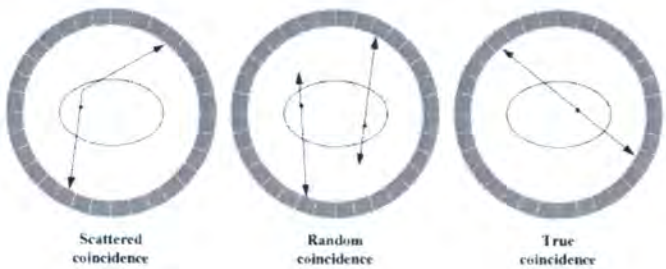

Figure 1.3: Types of coincidences in PET [13]

In the figure, • is the annihilation event; ⟶ is the gamma ray; and – – – is the assigned Line of Response (LOR) [13].

Random or accidental events are the events that occur if two signals arising from separate annihilations are detected within the same coincidence time window [14]. Scatter events are events that happen when one or both of the γ photons from a single annihilation event are scattered, but both are still detected. Since the random coincidence and the scatter coincidence (Figure 1.3) result in misplaced line of response, they also reduce contrast. The energy signals are sent to energy discriminators to reject events where the energy is not 511 keV. This rejection is however not very precise in a system optimized for time resolution [1].

For a three dimensional (3D) image, coincidences must be allowed to be detected between rings of detectors as well as within a ring of a detector. 3D techniques have better sensitivity (because more coincidences are detected and used) and therefore less noise, but are more sensitive to the effects of scatter and random coincidences, as well as requiring correspondingly greater computer resources.

1.2.3 Image reconstruction

The computer analyzes the γ-ray data and uses the information to create an image map of the object, for example, being studied. The image that represents the isotope concentration depends on the physics of positron decay, positron annihilation, γ-ray interactions in the object, and γ-ray detection, as well as the geometry and the engineering of the imaging system. The physical configurations of PET systems are designed to maximize the detection of coincidence events, and minimize background events from scattered photons, while minimizing high count rate from activity outside the field of view.

The event can occur anywhere in the tube which connects the two detectors. There are several ways in which the image can be reconstructed, this can be done through iterative reconstruction, back-projection and forward projection methods. A reconstruction algorithm uses the parallel projection $p(\rho, \theta)$ to construct an image of the tracer distribution f(x,y). Parallel projections are all sets of line integrals which intersect the tracer distribution at the same angle but different positions. The projections $p(\rho, \theta)$ approximate a line integral through a tracer distribution at a particular angle θ and a given distance ρ from the origin. In PET, most of the reconstructions of images are based on back-projection because an estimate of the original source distribution may be obtained. In back-projection, the magnitude of each value in a projection is added to every point in image space corresponding to the relevant line of integration in object space [13].

Back-projection thus convolves any function f(x,y) with 1/r and as a result any images of the tracer radioisotope using this method distort the image severely and thus another method needs to be used to remove or reduce the distortions. The filtered back-projections (Convolution back-projections) are utilized.

In filtered back-projection, the aim is to reduce the distortions of the image such that the parallel projections are filtered and then back-projected. When the convolution theorem is applied the functions become the multiplication of the Fourier Transform.

Since the image of the filter function can be changed to allow as much or little image blurring to remain in the picture as desired, different filter functions can be chosen to emphasize image edge detail or image density changes. Edge enhancement also emphasizes noise content while density enhancement minimizes image graininess and diminishes the amount of edge sharpness [15].

Forward projection is a reconstruction method that uses the information collected and plots a graph using the line of responses (LORs). This method is reconstructed by using multiple pixels, which are obtained from the construction of multiple LORs on to a grid. Every square on this grid presents a pixel. A disadvantage of using this method is that there is a lot of noise and the image is not of a good quality.

1.3 Kimberlite, the mineral to be searched for diamond

Figure 1.4: A Kimberlite Rock

Kimberlite is a grey-blue, dense, often altered and fragmented, intrusive igneous rock or extrusive igneous rock that contains the only diamonds known to occur in the rock matrix where they originally formed. Igneous rocks are formed when magma cools and solidifies, with or without crystallization, either below the surface as intrusive rocks or on the surface as extrusive rocks. This magma can be derived from partial melts of pre-existing rocks from either the earth's mantle or crust. The melting is caused by an increase in temperature, a decrease in pressure, or a change in composition. Igneous rock is classified according to mode of occurrence, texture mineralogy, chemical composition, and the geometry of the igneous body [16].

Kimberlite occurs in the earth's crust in vertical structures known as kimberlite pipes. Kimberlite pipes are the result of explosive diatreme volcanism from very deep mantle derived sources. Kimberlite are found as dikes and volcanic pipes which underlie and are the source for rare and relatively small explosive volcanoes. A dike is a tabular intrusive igneous body and its high angle is near vertical in orientation.

Not all kimberlite is diamond bearing, so it is necessary to evaluate its diamond content, and if there are diamonds, the size and the quality of the diamonds.

1.4 Problem Statement: Research and development of Mineral-PET

The ability to sort diamondiferous from barren kimberlite would result in much less processing and equipment required in the diamond mining industry. Unnecessary processing of the barren particles results in a large increase of the load and capacity required of the downstream processing equipment. This leads to an increase in the use of large equipment and considerable energy consumption, as the kimberlite rocks have to be processed and crushed to small pieces.

The purpose of Mineral-PET is to reject the barren kimberlite particles and continue processing only those particles which are indicated as diamond bearing materials.

An analytical model for the feasibility of the Mineral-PET system has been developed [1]. The model depends on several assumptions and parameters. This dissertation makes a study of several sectors of the model, and develops an improved set of parameters for these sectors, as well as improved understanding of the physics of these areas.

The Mineral-PET process has an activation stage and a detection stage. The activation stage is to generate the ^{11}C PET isotope in the kimberlite. The detection stage is where the occurrence of hot-spots in the PET signal may distinguish a diamondiferous from a barren kimberlite.

This dissertation makes a contribution in the detection part. Specifically, the evaluation of the absorption of 511 keV photons in the kimberlite (measuring and calculating the absorption length

of a typical kimberlite), and the impact of high count rates of both PET and non-PET isotopes in the signal-to-noise level of the PET detector system.

This has led to the following two studies:

- A study of the absorption length of the gamma ray attenuation in kimberlite material.
- A study of the ability of the coincidence condition in the detection system to reduce noise in the context of high count rate of both PET and non-PET isotopes.

Both of these items are crucial inputs to the PET analytical feasibility model.

Computer modeling by the Monte Carlo method is also used to determine whether the Mineral-PET detection system can identify the presence of possible diamond inclusion within the kimberlite rock. Monte Carlo simulation is the leading method for studying radiation transport and interaction in materials.The simulation can be used to understand the efficiency of the Mineral-PET process.

The Monte Carlo model of the Mineral-PET process also depends on the data from the absorption length measurement results of the first part of this study.

1.5 Objectives

As stated above, one of the aims of this project is to study the absorption length of gamma photons in the kimberlite. This part of the study had three approaches:-

- experimentally,
- theoretically using an analytical expression, and
- theoretically using a computer model by Monte Carlo simulation

The absorption length of the kimberlite was determined for a single detection system using the DART acquisition system (experimentally). The theoretical study using analytical expressions was based on tabulated data and an empirical gamma attenuation formula. The theoretical study using the Monte Carlo simulations was based on describing the geometry and the materials used

and then tracking the photon histories from a source, through the sample to a detector. The data for the absorption length of the kimberlite rock was determined in order to validate the Monte Carlo simulation performed using the GEANT4 code and to calculate the radiation length of the 511 keV photons in the kimberlite. These studies would later form part of the general feasibility calculation and also part of a more extended GEANT4 simulation of the entire Mineral-PET detector system.

The second part of the study was based on timing measurements to evaluate the random coincidence background contribution from the timing spectrum. The apparatus used consisted of an electronic CAMAC multi-parameter data acquisition system, the detectors and the sodium-22 (^{22}Na) radioactive source of coincident back-to-back 511 keV annihilation photons. The detectors were inorganic crystal scintillators mounted on photomultiplier tubes. Both very fast BaF_2 crystals and slower NaI (Tl) crystals were used. The results were interpreted using an analytical model and a Monte Carlo simulation. This validated the model for evaluating the effects of the random coincidence rate and gave strong evidence that the Mineral-PET system would be able to discriminate very well in favor of true PET events.

1.6 Thesis outline

Chapter Two explains the physics process and the feasibility study of the Mineral-PET system.

Chapter Three explains the experimental techniques including the absorption length measurement, time coincidence measurement, the set-up for Mineral-PET detector and the high-speed multi parameter event-by-event Data Acquisition system and the radiation safety in the laboratory.

Chapter Four presents the Monte Carlo methods, applications of the GEANT4 simulation, tube reconstruction and the 3D tube density distribution simulation and the scintillation simulation.

Chapter Five presents the results and analysis of this work. It compares the data from literature, experiment and the simulation.

Chapter six presents conclusion of the study, the findings and the challenges.

Chapter 2

Physics process and feasibility study of the Mineral-PET system

2.1 Introduction

The kimberlite rocks have to be activated with high-energy γ photons at the Giant Dipole Resonance (GDR) energy of carbon (a very broad peak centered at 22.5 MeV) for a short period in order to achieve the production of positron emitting isotopes, which serves as the basis for identifying the presence of possible diamond inclusions within the kimberlite rock.

A preliminary requirement for the process of γ irradiation is the crushing of the kimberlite rocks to pebbles of less than 10 cm in diameter. This is done to reduce the thickness of the material so that radiation can penetrate during the detection stage of the process, considering the absorption of the 511 keV photons which can greatly reduce the detection efficiency of these photons [18].

The activation process is used to transmute the carbon nucleus by a photo nuclear reaction, so that a daughter isotope emits signature radiation, which may be detected to indicate the presence of carbon. A linear accelerator must be used at this stage to activate the kimberlite rocks in order to enable the coincidence detection process in a later stage. An intense electron beam with energy of about 40 MeV, incident on a thick (about 1.5 mm) metal target (tungsten) is used to produce the Bremsstrahlung photons. When an electron of certain energy is incident on an atom and travels through the electric field of the nucleus of the atom, the electron loses energy in the form of photons, in a process called Bremsstrahlung. The shape of the energy spectrum of Bremsstrahlung photons is approximately proportional to 1/E. The photons of interest to the Mineral-PET technique

are in the range of 20 to 30 MeV where the (γ,n) reaction for the ^{11}C has a broad resonance. The kimberlite rocks are bombarded with a Bremsstrahlung radiation in order to produce the ^{11}C isotopes.

Figure 2.1 shows the yield in red from a GEANT4 Monte Carlo simulation for the production of photons from electron Bremsstrahlung using a 1.3 mm tungsten target bombarded by a 50 MeV electron beam. The blue line shows the region of the (γ,n) resonance reaction for the production of ^{11}C with a peak cross section of 8 mb (milli-barn)[1].

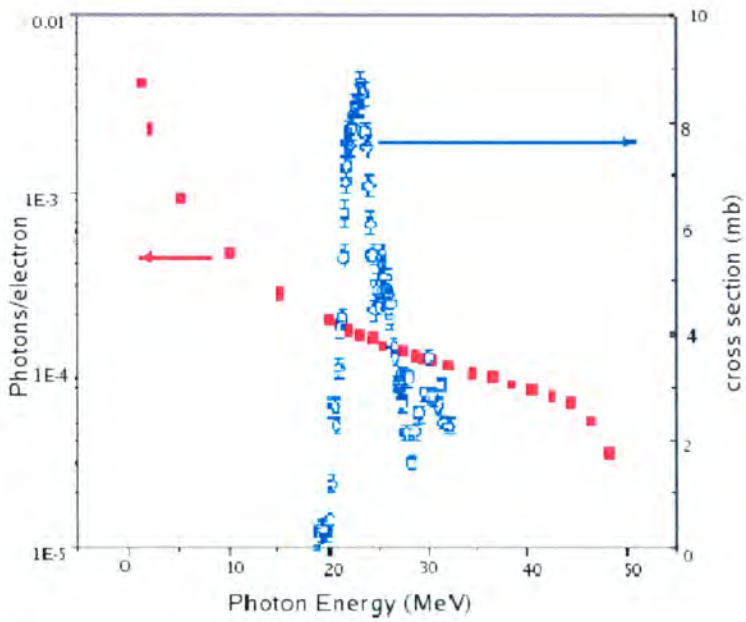

Figure 2.1: Photon activation of PET isotopes in kimberlite [1]

The Bremsstrahlung photons can activate many elements besides the required carbon. The elements in kimberlite may after irradiation cause interference during the detection process and contribute to a large background of γ-rays. Most of these radionuclides have very short half-lives as presented in Table 2.1. Other PET isotopes produced by the irradiation process have significantly different life-times.

The oxygen isotope (^{15}O) deserves special attention as it is also a PET isotope and it will lead to two back-to-back 511 keV photons. Oxygen is homogeneously distributed in the kimberlite, while carbon is concentrated almost exclusively in the diamonds, and ^{15}O has a much shorter half-life of approximately 2 min, compared to ^{11}C with its 20 min half-life. Allowing sufficient time before

the detection process, the positron emission activity of ^{15}O can be reduced to a level that is similar to or less than that of homogeneously non-diamond carbon (present in certain minerals within the kimberlite breccia) in the kimberlite. After about 20 min (10 half-lives) the oxygen isotope would have lost activity by a factor of 1/1000. At this stage, the dominant local concentration of PET activity would be the ^{11}C from a diamond, if it was present. The diamond identification can then proceed by detecting a statistically significant localization of PET emitters in a homogeneous background of PET emitters.

Kimberlite comprises a rich abundance of elements. Table 2.1 gives a presentation of the half-lives of the composite elements in the kimberlite rock that will be activated by the irradiation of kimberlite to determine the significant hot spot of localised carbon isotope (carbon in diamond form is spatially localized).

Radiation experiments on kimberlite have confirmed that only short half-life isotopes are generated in the activation process [1], as presented in Table 2.1.

Table 2.1: The Half lives of the Elements in kimberlite [1]

Si	^{24}Si-0.1s	^{25}Si-0.2s	^{26}Si-2.2s	^{27}Si-4.1s	-
O	^{13}O-8.9ms	^{14}O-7.1s	^{15}O-2m	-	-
Ti	^{41}Ti-0.8ms	^{42}Ti-0.2s	^{43}Ti-0.5s	^{24}Ti-3.1h	-
Al	^{22}Al-70ms	^{23}Al-0.5s	^{25}Al-7.2s	^{26m}Al-6.3s	^{24}Al-7e5y
Fe	^{49}Fe-0.1s	^{51}Fe-0.3s	^{52m}Fe-46s	^{52}Fe-8.3h	^{53}Fe-8.5m
Mn	^{49}Mn-0.4s	^{50m}Mn-1.7m	^{50}Mn-0.3s	^{51}Mn-46m	^{52m}Mn-21m
Mg	-	-	-	-	-
Ca	^{36}Ca-0.1s	^{37}Ca-0.2s	^{38}Ca-0.4s	^{39}Ca-0.9s	-
Na	^{20}Na-0.4s	^{21}Na-22s	^{22}Na-2.6y	-	-
K	^{35}K-0.2s	^{36}K-0.3s	^{37}K-1.2	^{38}K-7.6m	^{340}K-1e9y
H	-	-	-	-	-
P	^{28}P-0.3s	^{29}P-4.1s	^{30}P-2.5m	-	-
C	^{9}C-0.1s	^{10}C-19s	^{11}C-20m	-	-
Ni	^{53}Ni-0.1s	^{55}Ni-0.2s	^{57}Ni-36h	-	-
Cr	^{45}Cr-0.1s	^{46}Cr-0.3s	^{47}Cr-0.5s	^{48}Cr-22h	^{49}Cr-42m
Sr	^{79}Sr-2.1m	^{80}Sr-1.8m	^{81}Sr-22m	^{83}Sr-1.4d	-

2.2 Beta decay

The γ photons will interact with the carbon atoms of the material (amongst other atom types), transmuting carbon-12 to one of its radioisotopes, the carbon-11 nucleus. This is a positron-emitting isotope and has a half-life of approximately 20 min. The nuclear reaction is presented below:

$$^{12}C(\gamma, n)^{11}C.$$

This is followed by β decay of the carbon-11 nucleus:

$$^{11}C \Rightarrow^{11} B + e^{+} + \nu.$$

The carbon-11 nucleus decays by emitting a positron which thermalises in matter before annihilating with a neighboring electron. The result of this annihilation is (often but not always) to release two back-back γ-photons of 0.511 MeV each. The reaction is:

$$e^{+} + e^{-} \Rightarrow 2\gamma(511keV)$$

2.2.1 Physical process of β decay

β particles are fast electrons or positrons produced in the weak interaction decay of neutrons or protons in neutron or proton rich nuclei. The β process can decay via positive β decay (β^{+} decay) and negative β decay (β^{-} decay).

In β^{-} decay, a neutron decays into a proton, an ordinary electron and antineutrino. The daughter nucleus will have one proton more than before and thus the atomic number increase by one. The reaction is:

$$n \Rightarrow p + e^{-} + \upsilon'$$

In β^{+} decay, a proton decays into a neutron, positron and neutrino. The daughter nucleus will have one neutron more and the atomic number will decrease by one. The reaction is:

$$p \Rightarrow n + e^{+} + \upsilon$$

where υ is the neutrino; n is a neutron; p is a proton; e^{-} is an electron; e^{+} is a positron; and υ' is an

anti-neutrino [18].

2.3 Annihilation radiation

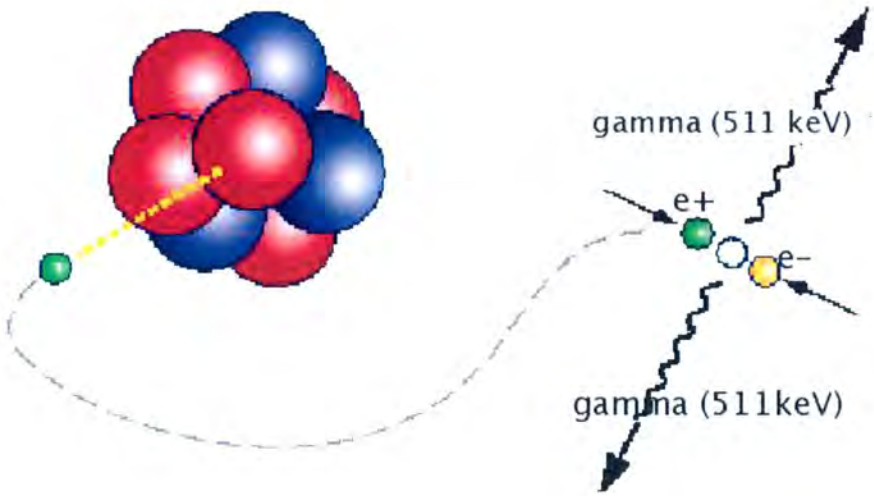

Figure 2.2: Annihilation radiation

The positron is an anti-electron that after travelling a short distance, will combine with an electron from the surroundings and annihilate. The positron annihilates with the electron to produce two photons, each with energy of 511 keV. In annihilation, the masses of both the electron and the positron are converted to electromagnetic radiation. In order to conserve energy and linear momentum, the electromagnetic radiation is in the form of two γ-rays (this is the most probable decay) of equal energy of 511 keV, which are emitted at 180^0 to each other. The photons are the quantum of the electromagnetic field.

The annihilation radiation is used to measure the quantity and the location of the positron emitter. The accuracy of the localization in PET depends on the physical size and the cross sectional geometry and of course on the position resolution of the detectors. The advantages for the localization of the positron emitter inside an object is that the two γ-rays are created simultaneously. The simultaneous or coincidence detection of two photons by the detectors on opposite sides of an object places the site of the annihilation on or about a line connecting the centers of the two detectors. The line is actually a tube when considering the position resolution of the system.

If the annihilation originates outside the volume between the two detectors, only one of the photons can be detected, and since the detection of a single photon does not satisfy the coincidence condition, the event is rejected [19].

The γ-ray interacts with matter in three main processes (for the MeV region of photon energy) namely photoelectric effect, Compton scattering and pair production. For 511 keV photons, pair production is not possible and so only the first two processes are significant.

The photoelectric effect occurs in the vicinity of an atom where the photon's energy is absorbed completely by releasing an electron; ejecting it from its site in the material. The full energy of the photon is passed on as kinetic energy of the electron, with a small correction for the binding energy of the electron. It is this energy that is then deposited into the detector.

In Compton scattering the scattered electron has less energy than the original γ photon while the energy of the electron resulting from the photoelectric absorption is much closer to the energy of the scattered photon; differing only by the binding energy of the photo-electron [20].

2.4 Photo-nuclear activation of PET isotopes in kimberlite

The activation process for $^{12}C(\gamma,n)^{11}C$ using Bremsstrahlung photons has been modeled with the Geant4 Monte Carlo code to determine the optimal combination of electron beam energy, electron beam current, and Bremstrahlung target thickness for conditions appropriate to Mineral-PET. The quantity that has been optimised is the power efficiency, defined as the number of photons on target, with energy in the Giant Dipole Resonance (GDR) region, per primary (beam) electron, normalised to the relative beam power of about 40 MeV. By simulating many different combinations of electron beam energy, current, Bremsstrahlung target material, and thickness, it was observed that the power efficiency tended to a plateau after about 40 MeV for the electron beam energy, for the most technically sensible choice of high-Z target, which was tungsten. The irradiation electron beam energy of 40 MeV onto 3 mm tungsten will therefore be assumed in what follows.

The activity from carbon-11 in a diamond in the kimberlite is related to the irradiation parameters as follows [1]:

$$A(t) = [t_\gamma N_{12_C}(e^{-x/X_o})(\phi_{e^-} 1/\Delta E \int_{\Delta E} P_{e^-\rightarrow\gamma}(E)\sigma_{(\gamma,n)}(E)dE)]\lambda_{11_C} e^{-\lambda_{11_C} t_h} \quad (2.1)$$

where t_γ is the time of irradiation; N_{12_C} is the number of carbon nuclei in a diamond of a given size; $e^{-x/Xo}$ is the attenuation of the irradiation photons in the kimberlite host matrix; X_o is the absorption length of kimberlite; ϕ_{e^-} is the electron flux from the Bremstrahlung target; $P_{e^-\rightarrow\gamma}(E)$ is the probability of an electron emitting a photon in the energy region of interest for the GDR process, $\sigma_{(\gamma,n)}(E)$ is the cross section of the Bremstrahlung and (γ, n) process respectively; E is the photon energy; ΔE is the energy range where the GDR region is significant; and $e^{-\lambda_{11_C} t_h}$ accounts for the decay of the ^{11}C during the waiting time in the hold hopper [1].

Typical parameters for run of mine production are throughput of kimberlite ore of 1000 tons per hour, with a belt speed of 2 m/s. Our calculations will assume approximately 1 sec for irradiation and 1 sec for detection. The aim is to determine the average beam that the electron accelerator will deliver on the Bremsstrahlung target (at an average of 40 MeV) in order to generate the flux of photons sufficient for the activation level required. The requirement is to find a 1 mm diameter diamond with at least 80% confidence limit.

It will be seen that the requirement sets the number of PET photons that must be detected compared to the background for a certain minimal size of diamond. For a given size and efficiency of detector, this becomes a requirement of the level of activation of the PET isotopes, which in turn sets the irradiation parameters. Considering the subset of the irradiation parameters given above as fixed, we must find the correct flux of photons or alternatively the electron beam current. This is discussed in more detail below.

2.5 The Mineral-PET algorithm

The kimberlite rock which has been pre-crushed to a coarse size of 10 cm diameter will be activated with a linear accelerator for a short period. After activation, the kimberlite rock will be placed into a 20 min hold hopper to eliminate interference from oxygen by allowing oxygen time to decay out. The non-diamond carbon is assumed to be homogeneously distributed in the kimberlite rock, whereas the Mineral-PET algorithm is looking for a diamond signal which will be a significant hot spot of localised carbon. The diamond sources of carbon are expected to be much more localised than the non-diamond sources.

The dual planar PET array of the position sensitive detectors will be placed on top and below the conveyor belt, which is used as a transport system containing kimberlite. The kimberlite rock of about 10 cm in diameter will be moving with a speed of 2 m/s on the conveyor belt between the detectors for data collection.

The actual size of the inclusion and its approximate location are derived from a statistical treatment of the intersections formed by reconstruction of the many tubes representing the correlated two photon trajectories from many decay events. The algorithm has to operate sufficiently fast for real time processing of rock in a conveyor belt situation.

The position sensitive detectors will detect the relative position and the actual size of the possible diamond inclusion within the kimberlite. Position sensitive detectors and the high speed multi parameter event by event DAQ system are used to gather signals from measurement sources and digitize the signals for storage, analysis and presentation in a computer.

2.6 Tube reconstruction and the 3D tube density distribution histogram

The computer analyzes the γ-ray data and uses the information to create an image of the tube reconstruction. The image that represents the tube reconstruction depends on the physics of positron emission, positron annihilation, γ-ray interactions in the object, γ-ray detection, as well as the geometry of the imaging system. The physical configurations of the Mineral-PET system are designed to maximize the detection of coincidence events, minimize background events from scattered photons, minimize high count rate from activity arising outside the kimberlite ore and to minimize the activity arising from non-diamond carbon.

Activated PET isotopes in the diamond and in the kimberlite will emit positrons that annihilate by emitting two back-to-back 511 keV photons at the same time and at some position to interact eventually with the detector. From the two opposite positions or points given by the detection of the pair of photons, a line is created, which is called a tube, because of the finite spatial position resolution of approximately 5 mm.

Position resolution for photon detection is the minimum detectable displacement of a spot light

incident on a position sensitive detector surface. The resolution is limited by the localization of energy deposition that spreads by Compton scattering as well as by the light collection process. The amount of scattering in the crystals depends on the γ-ray energy, the crystal stopping power and its thickness. For this process a conservative value of 5mm for the voxel size has been estimated.

The tube density distribution is therefore a 3-dimension histogram with a voxel size given by the position resolution of the system. To obtain a good identification, the volume of interest must be divided into voxels (volume pixel), and the tubes must be drawn into the voxels in the three-dimensional space (3D). A three-dimensional histogram is incremented tube by tube to generate a tube density distribution. Two or more tubes may intersect in a given voxel, and the number of tubes intersecting in that voxel is integrated to give a value for that voxel. The resulting three-dimensional histogram will contain events originating from real intersections from positron emitting isotopes in the diamond, and the real and false intersections (Figure 2.3) from the non-diamond carbon, and also from other sources of events in the tube density distribution. The false intersections are recorded when two tubes from the separate annihilation event intersect by chance away from their source points.

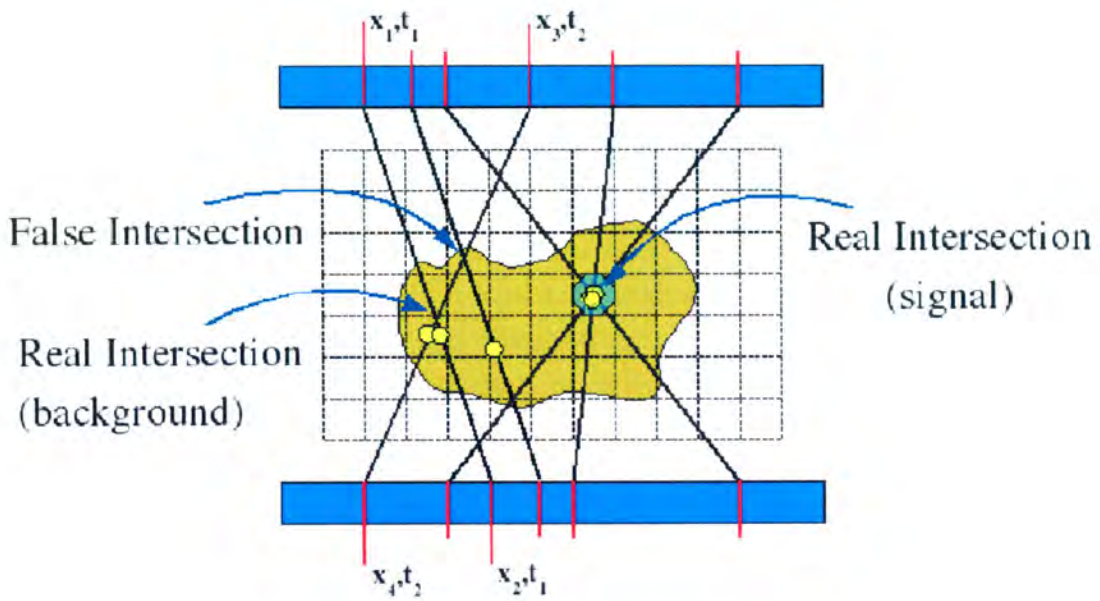

Figure 2.3: Tube Reconstruction

2.6.1 True intersections

Where two or more tubes intersect in the kimberlite at a common PET isotope rich source point, which indicates the presence of possible diamond inclusion, then the signal is the real tube intersections (Figure 2.3) from the diamond.

When there are many intersections of tubes, that indicates the presence of possible diamond inclusion within the kimberlite rock, Equation 2.2 presents the number of real intersections expected from diamond, based on the activity of the diamond and the efficiency of the detection system.

$$N_{\cap} = \varepsilon^2 \times \Delta\Omega/4\pi \times \Delta t \times A(t = 20min) \tag{2.2}$$

where $N_{\cap}$ is the number of real intersections from the PET isotope in the diamond; $\Delta\Omega/4\pi$ is the solid angle; Δt is the detection period; A is the activity of the diamond; and ε is the efficiency of each detector in the dual detection system.

All the diamond tubes will lead to a real intersection incrementing the 3-dimensional histogram, as the diamond size is almost always expected to be smaller than the voxel size.

2.6.2 False intersections

The background may result from the real intersections due to non-diamond carbon or remnant oxygen and also false intersections from random coincidences (Figure 2.3). The background leads to an incrementation of voxels in the 3-dimensional histogram, because of the statistical probability of intersecting with other tubes somewhere in the detection volume not located at the true source point of both tubes.

If u^3 is the total number of voxels in the detection volume, then the probability of any given voxel being incremented is

$$p = \frac{1}{u^3}$$

And if the number of tubes expected from non-diamond carbon is N, with a tube on average incrementing u voxels, then Nu events must be distributed over the 3-dimensional histogram. Therefore

the average number of background intersections per voxel will be:

$$B = \frac{N}{u^2} \tag{2.3}$$

The incremented contents of a given voxel containing a diamond is therefore

$$N_{voxel} = N_{\cap} + B \tag{2.4}$$

Where the statistical significance of a peak $N_{\cap}$ above the background is as follows:

$$\frac{(N_{voxel} - B)}{\sqrt{N_{voxel} + B}} \tag{2.5}$$

in the units of the Poisson variance of the peak counts.

2.6.3 Minimum Activity Required

In the worst case scenario, the quantity B is related to the quantity $N_{\cap}$ by assuming a minimum detectable diamond size (the 1 mm diameter diamond mentioned previously as the industry requirement) and a typical non-diamond carbon and oxygen content in the kimberlite composition. If the hold hopper eliminates the interference from oxygen, then this means a specific amount of non-diamond carbon and a minimum size for the diamond. A typical value assumed for the non-diamond carbon in the form of the CO_2 molecule is 0.2%. It is also assumed that the hold hopper brings the activity from the oxygen to less than the activity from the non-diamond carbon. For a kimberlite rock of about 10 cm in diameter, the amount of non-diamond carbon can be calculated and compared to the amount of the diamond form of carbon for the case of a 1 mm diamond in a kimberlite. (In this calculation, the density of kimberlite was used as 2.8 g/cm^3 and the density of diamond as 3.5 g/cm^3).

If considering one kimberlite rock containing 1 mm diamond, and the number of tubes detected from this diamond as $N_{\cap}$, then the relative amount of background to signal events will be

$$N = K \times N_{\cap} \tag{2.6}$$

Where K is the ratio of mass of non-diamond carbon (represented by subscript NDC) to that of the

diamond (represented by subscript D),

$$K = \frac{M_{NDC}}{M_D}$$

where $M_D = V_D \times \rho_D = 0.001$ cm $^3 \times 3.5$ g/cm$^3 = 0.0035$g

and $M_{NDC} = V_{NDC} \times \rho_{NDC}$

where $\rho_{NDC} = P_{NDC} \times \rho_k$, P_{NDC} is the weight percentage of the non-diamond carbon

Considering the percentage of carbon dioxide in the kimberlite ($P_{CO_2} = 0.2\%$) from Table 2.1, and also the molecular mass of carbon and carbon dioxide:

$P_{NDC} = \frac{M_c}{M_{CO_2}} \times P_{CO_2} = \frac{12}{44} \times 0.2\% = 0.000545$

$\rho_{NDC} = P_{NDC} \times \rho_k = 0.00153 g/cm^3$

then $M_{NDC} = V_{NDC} \times \rho_{NDC} = 1000 cm^3 \times 0.00153 g/cm^3 = 1.53$g

$$K = \frac{M_{NDC}}{M_D} = 437$$

Equation 2.6 gives $N = 437 N_\cap$

Then substituting N from equation 2.3 gives:

$$B = \frac{437 N_\cap}{400} = 1.0925 N_\cap$$

Considering 1.6σ or 80% confidence limit,

$$\frac{N_\cap}{\sqrt{N_\cap + B}} > 1.6$$

Substituting $N_\cap$ and B, $N_\cap = 5.4$

The probability of n intersection events found in any particular voxel is a Binomial distribution or approximately a Poison distribution, as presented in the following equation.

Considering that $p = \frac{1}{u^3}$, so $B = \bar{n} = Nup$

$$P(n, Nu, p) = \begin{pmatrix} Nu \\ n \end{pmatrix} p^n (1-p)^{Nu-n} \approx (B)^n e^{-B}/n! \tag{2.7}$$

This justifies the $\sqrt{B}$ for the variance of B and $\sqrt{N_{voxel} + B}$ for the variance of $N_{\cap}$.
Therefore, considering a 1 sec measuring time in a 2 m long linear PET array for a conveyor belt moving at 2 m/s, and solid angle ($\Delta\Omega = 2\pi(1 - Cos\theta)$ where $\theta = 30^0$), the activity will be;

$$N_{\cap} = \varepsilon^2 \times \Delta\Omega/4\pi \times \Delta t \times A$$

Considering Equation 2.2, the efficiency of the detection system: $\varepsilon = 0.38$

Therefore, considering the parameters, the minimum activity for the diamond: $A = 551$ Hz.

2.6.4 Estimate on Feasibility

The electron flux of the bremsstrahlung can be calculated using Equation 2.1, as follows:

where the measuring time (t_γ) = 1sec

$$N_{12_C} = \frac{\rho}{M_r} \times N_A \times t$$

where the density of carbon-12 from the literature is $\rho_{12_C} = 3.5 g/cm^3$, N_A is avogadro's constant ($6.022^{23} mol^{-1}$), M_r is molar mass of carbon (12g/mol), and t is the thickness of 1mm diamond.

Then $N_{12_C} = \frac{\rho}{M_r} \times N_A \times t = 1.76 \times 10^{20} m^{-2}$

Considering the thickness of kimberlite material (x) as 10 cm diameter and the absorption length of kimberlite (X_o) as 9.3 cm, then $e^{-x/Xo} = 0.34$

$$\lambda_{11_C} = \frac{In2}{t_{1/2}} = 0.034/\text{min} = 0.00057/\text{sec}$$

Considering t_h as the 10 min delay period, then $e^{-\lambda_{11_C} t_h} = 0.71$

Considering fig 2.1, the probability (P = number of photons/electrons/energy bin = 0.09) and σ= 8mb, then:

$1/\Delta E \int_{\Delta E} P_{e^- \rightarrow \gamma}(E)\sigma_{(\gamma,n)}(E)dE = \sigma \times \int PdE = 7.2 \times 10^{-31} cm^2$

The activity from section 2.6.3 is given as 551 Hz

Therefore, considering the parameters, $\phi_{e^-} = 3.16 \times 10^{16} s^{-1}$

Therefore, calculating the current:

$$i = \frac{\phi_{e^-} \times Q}{t}$$

where Q is the charge ($q = 1.602 \times 10^{-19} C$) of the electron and t is the measuring time (t=1s).

Therefore, Current = $5.06 \times 10^{-3} Cs^{-1}$ = 5mA

The electron accelerator has to deliver on the bremstrahlung target a very high average beam of 5mA in order to generate the flux of photons sufficient for the activation required.

Chapter 3

Experimental Techniques

3.1 Absorption length

3.1.1 Set-up for absorption length

The main aim of this measurement was to determine the absorption length of the ^{60}Co γ photons in the kimberlite. Absorption length is the average length in a specific material in which a photon will lose a fraction of its energy by bremsstrahlung. The absorption length is an important data parameter for the full Monte Carlo simulation of the Mineral PET system, and a comparison of measured absorption length with a small Monte Carlo simulation was used to gain experience with GEANT4 and to test the Monte Carlo simulation.

The absorption length of the kimberlite was determined in three methods: firstly using a single detection system known as the DART acquisition system (experimentally), secondly using an analytical expression (theoretically), and thirdly using the Monte Carlo simulation computer model (theoretically).

The theoretical study using analytical expressions was based on tabulated data and the empirical γ attenuation formula. The analytical solution was achieved by using the formula for calculating the absorption length of a mixture of substances where the absorption length of the elements in the mixture is known. The numerical study using the Monte Carlo simulations was based on describing the geometry and the materials used and then tracking the photon histories from a source, through the sample to a detector. Aluminum was used as a reference to determine the reliability of these methods, since the absorption length is known to be 8.9 cm. Aluminum was also chosen because it

was readily available at the iThemba Laboratory of Accelerator Based Science (LABS) Gauteng. Ultimately the absorption length for kimberlite would be required.

The apparatus used to determine the absorption length of aluminum and kimberlite consists of a cobalt-60 (^{60}Co) radioactive source, a NaI (Tl) detector and the DART acquisition system.

^{60}Co is a radioactive metal, and it produces two γ-rays with energies of 1.173 MeV and 1.338 MeV. The ^{60}Co has half-life of 5.27 years, atomic mass of 58.9 g/mol and a density of 8.90 g/cm3 [21].

A slower NaI (Tl) inorganic scintillator mounted on a photomultiplier tube was used as a γ-ray detector. The NaI (Tl) detector provided an energy spectrum consisting of the full-energy peak, Compton edge, Compton continuum and backscatter peak (Figure 3.1) [22].

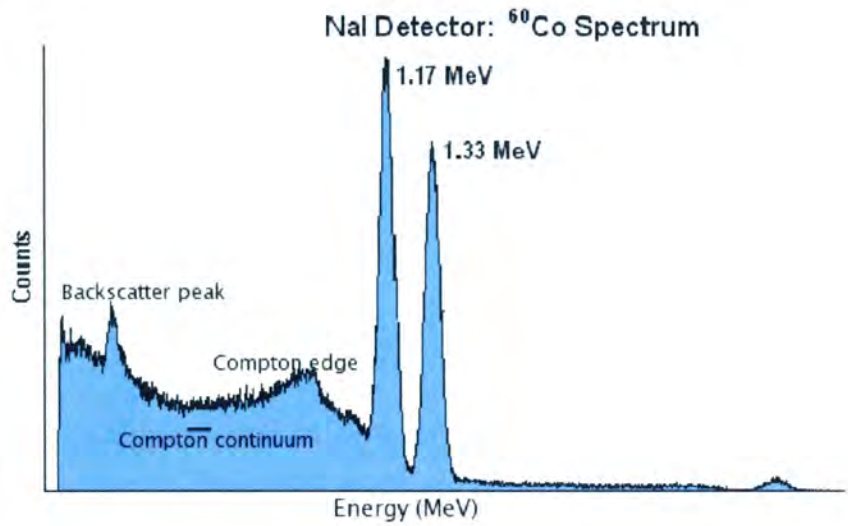

Figure 3.1: A spectrum of a ^{60}Co source with NaI (Tl) detector

The full-energy peak corresponds to events in which the γ-ray transfers all of its energy to electrons in the crystal. The fraction of the detected γ-rays that contribute to the full energy peak are very dependent on the size and the shape of the detector, the atomic number (Z) of the material, and the γ-ray energy (E_γ).

The Compton edge is the energy obtained as the maximum energy of the recoil electron.

The Compton continuum is due to the Compton scattering with the scattered γ-ray escaping undetected.

The backscatter peak is the peak that originates from γ-rays that are Compton scattered by surrounding materials through large angles back into the detector where they pass through photoelectric absorption.

The DART acquisition system is a combination of an Amplifier, High-Voltage supply, Analogue to Digital Converter and multi-channel analyzer that was used to transmit the spectrum to the computer for analysis, storage and presentation. The NaI (Tl) detector was connected to the DART system. An oscilloscope was used to monitor the signal from the detector and from the DART system.

An oscilloscope is a graph displaying device that draws a graph of an electrical signal. The graph is used to show how signals change over time. The vertical axis presents voltage and the horizontal axis presents time in seconds. This graph can assist in setting-up the instruments, and in determining how much of the signal is noise and whether the noise is changing with time. It can also be used to calculate the frequency of an oscillating signal, and find out how much of the signal is alternating current or direct current.

3.1.2 The procedure used to determine the absorption length of γ photons in kimberlite using the measurements

Measurements were done with both aluminum and kimberlite rock as absorbers. The absorber had a thickness of 1 cm. A ^{60}Co source was placed 10 cm away from the NaI (Tl) detector with the absorber in between. The control measurement was a similar set-up with only the source placed 10 cm away from the NaI (Tl) detector (no absorber). During data collection the same real time was selected for the measurements with and without absorber.

The representation from the Monte Carlo calculation used to measure the absorption length with an absorber is shown in Figure 3.2.

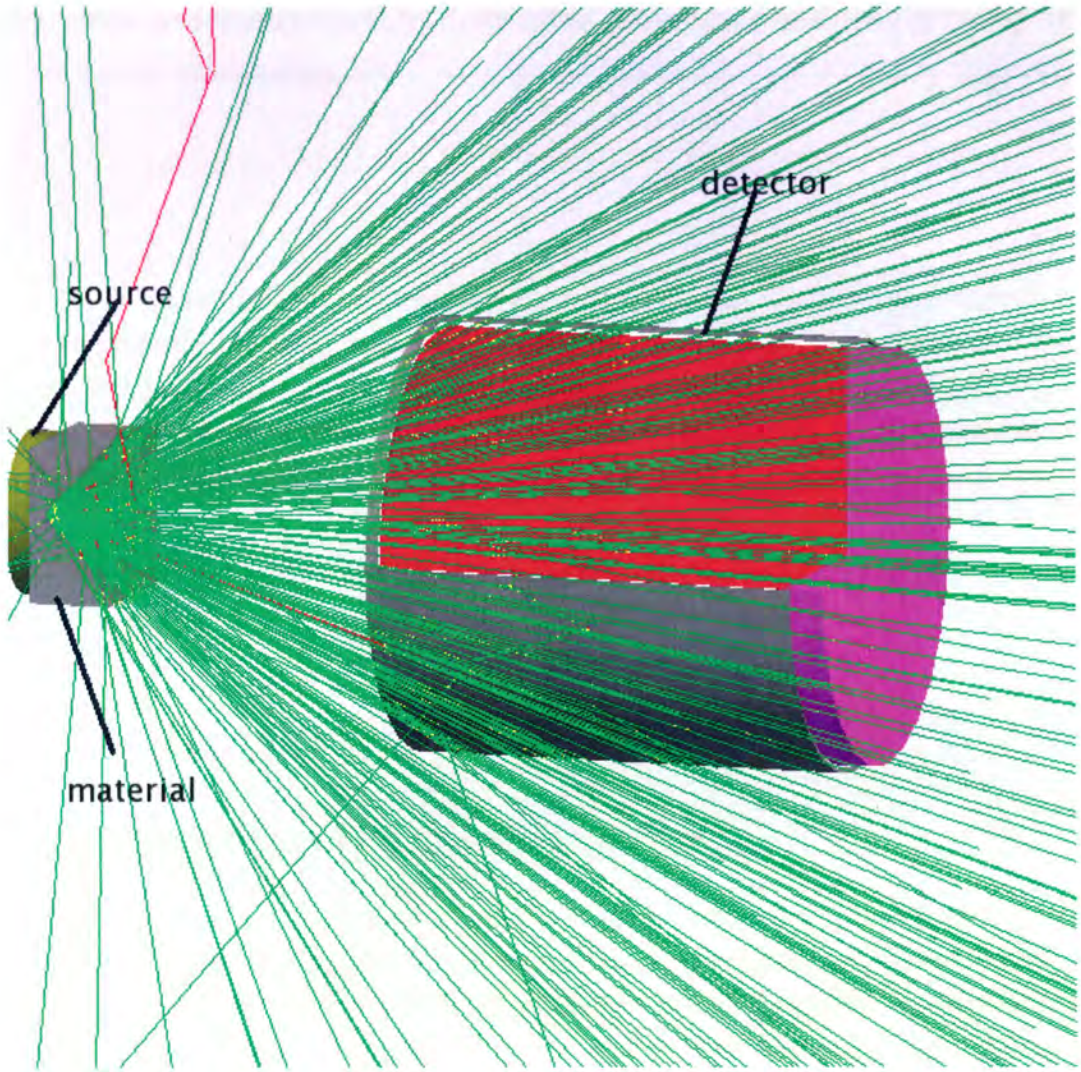

Figure 3.2: A representation from the Monte Carlo calculation of a ^{60}Co source placed 10 cm away from the NaI (Tl) detector with the absorber in between.

In the figure, the source is the ^{60}Co; green lines represent the photons from ^{60}Co; red lines represent electrons resulting from the photoelectric effect; the material is the kimberlite or aluminum; the detector is a NaI (Tl); the red colour in the detector represents the detector crystal; the purple colour in the detector represents the borosilicate glass (p hotomultiplier tube glass); and the grey colour in the detector represents the Teflon (wrapper for backscattering).

3.1.3 The procedure used to determine the absorption length using Monte Carlo simulation

A Monte Carlo simulation was used to determine the absorption length of γ photons in kimberlite and aluminum.

The set-up of the simulation measurement was similar to the experimental measurements. A ^{60}Co source was placed 10 cm away from the NaI (Tl) detector with the absorber in between as shown in Figure 3.2 . The control measurement was a similar set-up with only the source placed 10 cm away from the NaI (Tl) detector (no absorber). At the end of a certain number of events, a histogram was recorded.

The experimental and Monte Carlo simulation analysis and the results of the absorption length are presented in Chapter 5.

3.2 The Time Coincidence Measurement

3.2.1 Set-up for coincident timing measurement

The main purpose of the timing measurement is to extract the random coincidence rate from the real coincidence rate. It is necessary to perform a timing measurement, in order to establish that annihilation photons are in coincidence. When a detector absorbs a photon, an electronic pulse is generated with a width (τ), amplitude and a time relation to the absorption of the photon by the detector. The accuracy of the timing depends on the properties of the detector and the electronic instrumentation chain. The range of the gate for the timing signal is chosen to ensure that most of the signal from true coincidence will fall into the electronic coincidence time window. Because of the width of the coincidence time window, there is a probability that unrelated photons will accidentally produce timing signals that will pass through the detector and produce a random coincidence.

The apparatus used for this measurement consists of an electronic CAMAC data acquisition system, BaF_2 detectors and a sodium-22 (^{22}Na) radioactive source of coincident back-to-back 511 keV annihilation photons. The detectors were inorganic crystal scintillator mounted on photomultiplier tubes. The results were interpreted using an analytical model and a Monte Carlo simulation.

The ^{22}Na source was placed between the two detectors. The source was used to produce coincidence events in the two BaF_2 detectors. The ^{22}Na source emits a 1274 keV photon together with two 511 keV photons from positron annihilation all in coincidence.

The BaF_2 detectors have been chosen because of its very fast component in its scintillation decay. These detectors have high atomic number components with a decay time of less than 1 ns. The BaF_2 detectors are important in that they have both a high detection efficiency per unit volume and a fast response. The light yield in the fast components is quite small, only about 1400 photons per MeV. The fast timing capability coupled with the high density and the high atomic number of the material have made it the scintillation material of choice in timing measurements.

The electronic set-up used in the timing measurement is shown in Figure 3.3, where ^{22}Na is sodium-22 source; Det1 and Det2 are BaF_2 detectors; Rail represent detector alignment; HV is the High voltage Supplier (max HV = 2200V for BaF_2); CFD is the Constant Fraction Discriminator; TAC is the Time to Pulse Height Converter (TPHC or TAC); G&D is the Gate and Delay Generator; Quad Amp is the Quad Amplifier; RM is the linear rate meter; and SA is the Spectroscopy Amplifier.

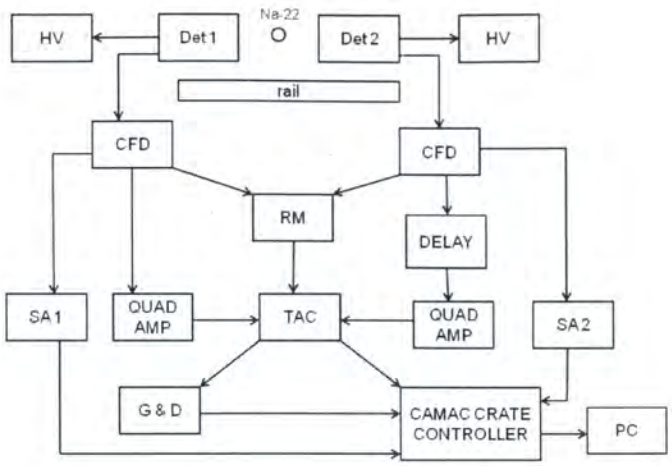

Figure 3.3: The logic diagram of the coincidence measurement.

The BaF_2 detectors and the ^{22}Na source were placed on top of a wood rail alignment, to ensure that the detectors are 180^0 to each other, and the source is pointed directly to both detectors.

A preamplifier of the BaF_2 detector shapes the analog signal from the detector. The anode signal from the detector was chosen for timing measurements. The short decay time of BaF_2 gives a good timing resolution. Since the direct output of the BaF_2 is sufficiently large, the detector output was directly connected to the Model 473A Constant Fraction Discriminator (CFD), from CFD to the Model 467 Time to Amplitude Converter (TAC) as the start signal, and in the same way, the signal from the anode of the second BaF_2 detector was fed via a Model 473A CFD through a delay module to the Model 467 TAC as the stop signal. The analog signal from TAC was sent to the Analogue to Digital Converter (ADC) in the CAMAC crate for digitisation and formation of the spectrum. The Spectroscopy Amplifier outputs were also sent to the ADC in the CAMAC crate. The CAMAC crate itself was gated by the logic pulse from Gate and Delay generated by the TAC indicating a valid measurement. This signal was correlated to the TAC output signal by use of a Model 416A Gate and Delay Generator.

The CFD produces the logic output pulses indicating the presence of a linear pulse within the range determined by the differential mode or merely exceeding the integral mode. Thus one can select

a range of pulse heights with this instrument. There is also an adjustment for the delay in the Constant Fraction principle. There is a lower energy-level discriminator and an upper energy-level discriminator which may be used to reject the pulses below and above particular values [23].

The delay module was needed since the first detector provided the early signal and the second detector provided the later signal. This shifts the coincidence time from zero to midrange of the TAC. This delay module has been chosen for the fast signal. The fast signal comes from pulses with rise time of less than nanoseconds used for time measurements, whereas the slow signal comes from pulses which have rise times of greater than nanoseconds used for energy measurements. The rise time is the time it takes for the pulse to rise from 10 to 90% of its full amplitude. The pulse rise time is dependent upon the scintillation decay time and on the collection and transit time characteristics of the PMT. The amplitude is the height of the pulse as measured from its maximum value to the instantaneous baseline below the peak. Since the detectors are placed face to face with the positron annihilation source (^{22}Na) between them, the fast delay module may be used to adjust the position of the coincidence peak.

This delay module provides adjustable delays which permit a lengthening or shortening of the electrical paths in a coincidence circuit. It is important to assure that the electrical paths along which two coincident signals travel to the coincident unit are equal except for the offset to move the coincidence peak into the centre of the TAC range [24].

The TAC or Time to Pulse Height Converter (TPHC) utilizes the fast negative logic outputs of the CFD's as input. The TAC analog output is proportional to the time interval between the start input and the stop input. TAC determines if two or more logic signals are coincident in time and it also generates a logic signal if true and no signal if false [24].

If the two signals are unrelated to each other, the time difference between them can take any value, and the TAC output can be any pulse height. But if the pulses bear a specific relation in time, then the TAC output will be a specified pulse height. This pulse height signifies all real coincident events and can be used to identify them. The width of the TAC pulse height distribution indicates the time resolution of the system [24].

The TAC module has an adjustable upper threshold (ULD) and a lower threshold (LLD), which define an acceptance window. The threshold should be adjusted so as to ensure that the electronic noise is eliminated [24].

An ADC was located after the TAC, to convert an analog signal to an equivalent digital word. The signal then gets read in by a CAMAC crate controller and is collected and displayed by a computer using software [24].

There is a time difference between the analog pulse (representing the time measurement) arising from a coincidence event and the logical signal to be used as an ADC gate signal. In order to deal with this, the timing pulses are passed to a gate and delay generator. The Gate and Delay Generator creates an electronic pulse after a present adjustable delay, and therefore it was located after the TAC. The Gate and Delay Generator is a triggerable device which generated a variable width gate pulses ranging from a few ns to as long as a few sec. This module was used to change a negative pulse to a positive pulse, and can also be used to change pulse width, height, and time. The Gate and Delay module ensured that the analog pulse from the TAC arrived at the same ADC at the same time, as the gate pulse arriving at the CAMAC Crate Controller.

The Data Acquisition (DAQ) system with P.C CAMAC interface [HYTEC 1331/TURBO] was used to gather the signal from measurement sources and digitise the signal for storage, analysis and presentation in a PC. The CAMAC system was designed to complement the NIM system for nuclear electronics and was designed simply as a standard system for the transmission of digital data. The CAMAC is a modular system, the essential components of which are a crate and plug-in type modules. The crate is composed of slots or stations in which the modules are inserted. At the rear of the module is a card-type connector which mates with a corresponding connector at the back of the slot [23].

The crate controller oversees all communication within a CAMAC crate. This crate can issue commands and is thus the master allowing digital signals to be transmitted to or from plug-in modules [24].

A linear rate meter was used to count the single rate from the single channel analyser (SCA) of the TAC, and also from the positive output of each CFD. The rate meter is a device, which instead of giving the number of counts and the time period in which those counts are collected separately, directly yields the count rate (counts/sec). A rate meter always has associated with it a parameter known as the time constant. The time constant of a rate meter determines the statistical accuracy of the count rate due to the averaging time, which also affects its response time to the changes in the count rate [24].

The two-channel storage oscilloscope with 1GH/s was also used to test the efficiency of the detector and the signal from the modules.

The analysis and the results of the time coincidence are presented in chapter 5.

3.2.2 The study of the random rate measurements

The study of the random rate was performed in order to obtain the random rate, to ensure that the random measurements are well understood. The timing measurements have shown that the rate of random coincidences is very low and hard to quantify on a short time scale of 100 ns. This indicates the enormous noise rejection power of the fast coincidence detection system. The experiments indicate that the important criteria of discriminating against the random coincidence of the γ photons in the region of 511 keV is the resolving time of the coincidence system.

The evaluation between the real coincidence and the random coincidence must be done at very high random rates in order to see the effects of the random rate clearly, whereas the experiment discriminated very well in favor of the true coincidences. The aim of this experiment was to extract the random coincidence from the real coincidence. In order to obtain sufficient random events, the measuring time was increased from 100 ns to 80 μs, and the detectors were placed 90^0 to each other as shown in Figure 3.4. This last step eliminated the real back-to-back coincidences, and the random coincidences are more visible.

The electronic set-up used in this measurement as shown in Figure 3.4 were arranged in the same way as used in the timing measurements (Figure 3.3), the only difference was the position of the BaF_2 detectors and the longer time range of the TAC.

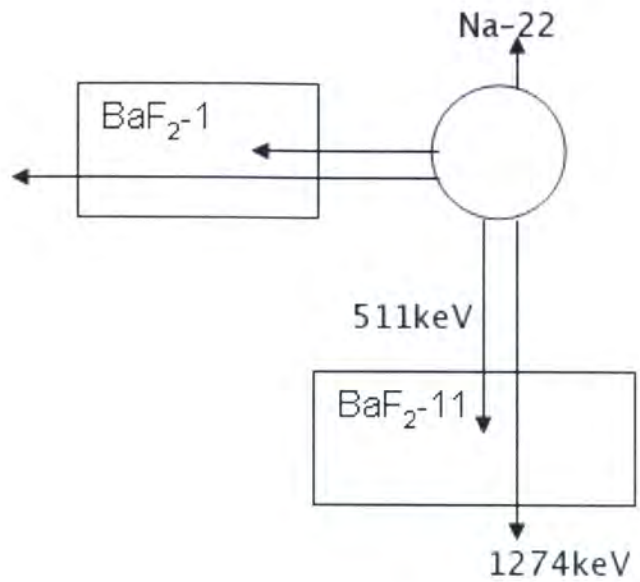

Figure 3.4: The logic of the random coincidence measurement

Since the detectors are placed 90^0 to each other, the annihilation originates outside the volume between the detectors, therefore only one of the correlated photons can be detected, and since the detection of only one correlated photon does not satisfy the true coincidence condition, only the random coincidence will be generated. Even if the detectors are placed 90^0 with 80 μs resolving time there is still a possibility that the coincidence peak can be generated because of the isotropic 1274 keV photon that is emitted together with the 511 keV in coincidence.

Each detector measured annihilation signals N_γ from the BaF_2 (γ-detector). Assuming that the detection efficiency of the γ-detector is ε_γ, where the N_γ was recorded.

The N_γ events from the first detector is

$$N_{\gamma_1} = \varepsilon \times \Delta\Omega/4\pi \times A \tag{3.1}$$

The N_γ events from the second detector is

$$N_{\gamma_2} = \varepsilon \times \Delta\Omega/4\pi \times A \tag{3.2}$$

where N_{γ_1} is the rate of events from the first detector; N_{γ_2} is the rate of events from the second detector; ε is the efficiency of the detection system; $\Delta\Omega/4\pi$ is the solid angle; and A is the activity

Therefore the rate of random coincidence N_r in a time interval Δt is,

$$N_r = (\varepsilon \times \Delta\Omega/4\pi \times A)^2 \times \Delta t \tag{3.3}$$

where Δt is the detector resolving time since these events are independent.

On the other hand, for correlated events, the rate of coincidence events N_c is,

$$N_c = \varepsilon^2 \times \Delta\Omega/4\pi \times A \tag{3.4}$$

The well known results indicate that true coincidences scale with activity, whereas the random coincidences scale with the square of the activity.

The waiting period between random events can be calculated. In case of the random rate, the waiting period is defined as the time interval between the start event and the stop event. Since the events are independent of each other, and supposing the radioactive source is observed with a mean rate λ, then the waiting period distribution should be represented by an exponential interval distribution in which the probability of an event occurring between time t and t+dt is P(t)dt, where

$$P(t) = \lambda exp(-\lambda t) \tag{3.5}$$

and λ is the singles rate = N_γ.

The analysis and the results of the random rate are presented in chapter 5.

3.2.3 The time calibration measurement

The main purpose of the time calibration measurement is to ensure that the electronics (TAC) used to perform time measurement are accurate and are dependable calibrated measurements. The electronic set-up used in the calibration measurement is shown in Figure 3.5.

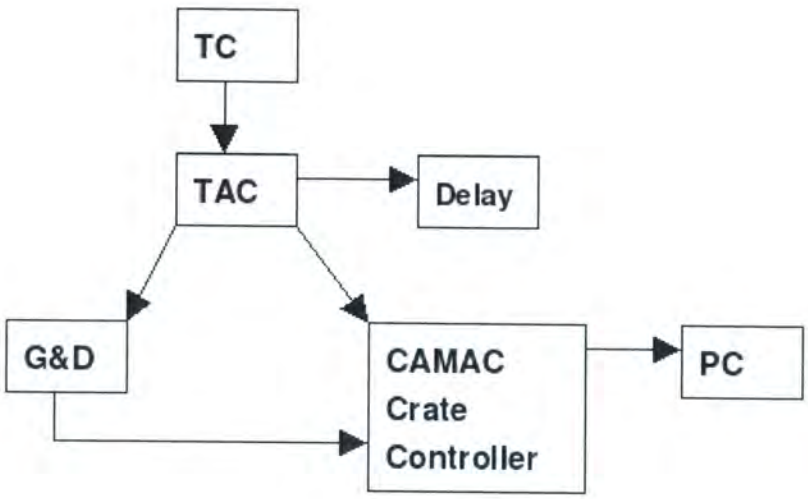

Figure 3.5: The logic diagram of the time calibration measurement

The analysis and the results of the time calibration are presented in chapter 5.

3.2.4 The Energy Measurement

The energies of the γ-rays were also determined in order to observe the 511 keV peak, the Compton peak, and the 1274 keV peak, and also to compare the energy spectra from both detectors with the time spectrum. The two measurements are related to two types of electronic pulses that can be observed, linear pulses and logic pulses. The linear pulses are defined as those pulses in which the signal amplitude is proportional to the parameter of interest (time or energy). By contrast, logic signals have a fixed shape and amplitude, and they convey information by their presence, absence or relation to time.

The electronic set-up used in the energy measurement was similar to the set-up shown in Figure

3.3.

In this set-up, the pre-amplifier converts the pulse from the PMT dynodes of the BaF_2 detectors to a voltage pulse using a variable capacitance. The dynode signal from the detectors was chosen for energy measurement, because it provides linear signals. Since the direct output of the BaF_2 is sufficiently large, the detector output was connected directly to the Spectroscopy Amplifier (SA). The energy signals of the detectors were shaped and amplified by the SA.

The amplified signals were digitized by the ADC in the CAMAC crate as controlled by the crate controller, to convert an analog signal to equivalent digital pulses. The data was then collected and displayed by a computer using the software [23].

The analysis and the results of the energy measurements are presented in chapter 5.

3.3 Set-up for Mineral PET detector and the high speed multi parameter event-by-event Data Acquisition

3.3.1 Introduction

Experiments were performed using a pair of detectors in a coincidence mode. The improvements in Mineral-PET require scintillation crystals with good imaging resolution for high light output, high sensitivity, fast rise and fast decay. They also require scintillation crystals with low cost for the mass production of large size crystals, high production yield and also others with stable performance and no internal radioactivity [23].

The detection systems are crystals that scintillate when any particle interacts. By combination of medium energy resolution and excellent time resolution, the coincidence of 511 keV photons that identify a positron annihilation can be extracted from the background of non-511 keV radiation with a signal to noise ratio of better than 99%. Even though the detectors are subjected to a high flux of radiation from the kimberlite mass, the granularity of the detector system and the large number of channels of the electronic data processing leads to rates of events per channel which are more than an order of magnitude below saturation. Granularity is the relative size, scale and level of detail that characterizes an object [1]. In this context it implies that the PET detector system has a large number of independent sub-detectors, so that the total rate is divided by many subsystems.

The detectors used in PET are inorganic scintillation crystals, which are used to record γ-rays produced by the annihilation of positrons emitted by the PET isotope. Inorganic scintillator are mainly crystals of alkali halides sometimes containing a small activator impurity, such as NaI(Tl), CsI(Tl), KI(Tl), with thallium (Tl) as the impurity activator. Among the non-alkali material are BGO, $CdWO_4$, $CaWO_2$, ZnO(Ga), ZnS(Ag) and BaF_2.

The advantage of inorganic crystals lies in their greater stopping power due to their higher density and higher atomic number which make them suitable for detection of photons and lead to better detection efficiency. A high detection efficiency for the γ-rays of interest requires both a high atomic number for a large photoelectron cross section and a high density for a large Compton scattering cross section. These are the two main interactions through which 511 keV γ-rays interact with the scintillator crystals as explained in Section 2.2. They also have some of the highest light outputs, which result in better energy resolution. This makes them suitable for the detection of γ-rays and positrons.

3.3.2 The scintillation detectors used in Mineral-PET

The γ photons in Mineral-PET were best detected with inorganic scintillation materials, for example bismuth germanate ($Bi_4Ge_3O_{12}$), also called BGO, thallium-activated sodium iodide (NaI (Tl)) and barium fluoride (BaF_2) (Table 1.2.2). Inorganic scintillators are crystalline solids that scintillate because of the characteristics of their crystal structure [25].

The scintillation crystals are coupled to PMTs that convert the light energy of photons into a timed electric pulse. The timed electric pulse is amplified and used to determine whether the two photons detected are coincident. The size of the pulse is proportional to the photon energy deposited in the crystal by the photon. The photons create an energetic electron by the photoelectric effect or by Compton scattering. As the photoelectron passes through the scintillator, it interacts with the scintillator and in turn it excites other electrons which, when they decay back to their ground state emit visible light [25].

3.3.3 Photomultiplier Tubes

A PMT is a light-sensitive device which converts visible light into measurable electronic pulses. It consists of a cathode made of photosensitive material followed by an electron collection system facing the window through which the light enters, a series of metallic electrodes known as dynodes, and finally an anode from where the final signal can be collected. All parts are usually housed in an evacuated glass tube. During operation a high voltage is applied to the cathode, dynode and anode such that a potential is set up along the length of the cathode through the dynode to the anode. When an incident photon hits the photocathode it produces an electron of low energy through the photoelectric interaction. Because of the applied voltage the electron is then directed and accelerated towards the first dynode, where it transfers some of its energy to the electrons in the dynode. This causes secondary electrons to be emitted, which are accelerated towards the next dynode where more electrons are released and further accelerated. An electron cascade down the dynode string is created. At the anode, this cascade is collected to give a current which can be amplified and analyzed. The gain of a PMT strongly depends on the voltage applied to a dynode and therefore on the high voltage itself [26].

The purpose of the PMT is the large area coverage at limited cost with high resolution, high detection efficiency, good energy resolution and fast time response.

3.3.4 A Bismuth Germanate detector

The preferred detector in Mineral-PET is BGO because of its higher atomic number and greater efficiency for the photoelectric conversion of γ-rays. The greatest efficiency of the BGO scintillation crystal (Figure 3.6) makes it suitable for detecting the position of the energy deposition in the material. Its mechanical and chemical properties make it easy to handle and use.

It is used in particle physics, nuclear physics, nuclear medicine and other industries. BGO has a good performance and is sufficiently dense to allow a small thickness that limits the parallax effects. Parallax is an apparent motion of an object against a distant background because of a perspective shift, and it can cause blurring.

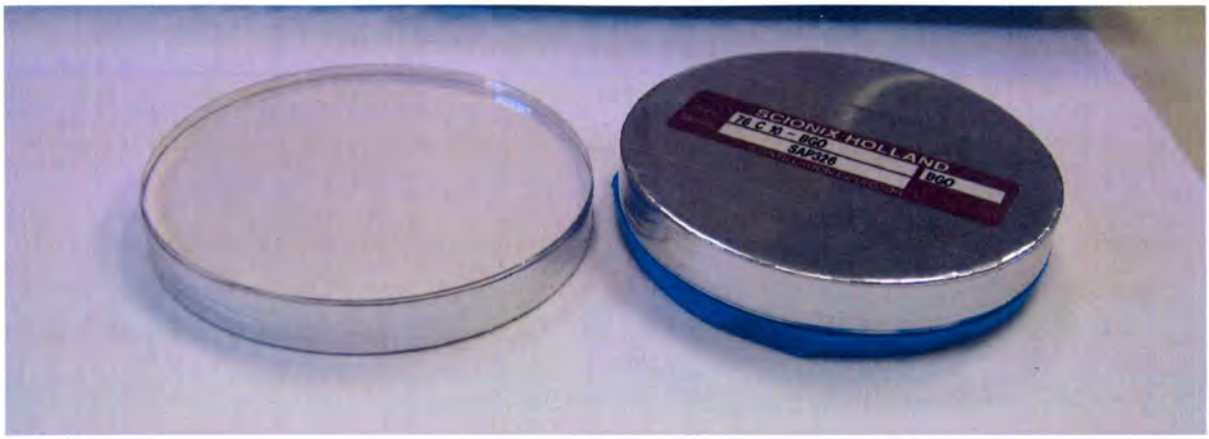

Figure 3.6: BGO Scintillation Crystal

3.3.5 Thallium-activated sodium iodide detector

NaI (Tl) has very good luminescence efficiency and is available in single crystal or polycrystalline forms in a wide variety of sizes and geometries. NaI (Tl) is used in nuclear medicine, environmental monitoring, high-energy physics and also in many other applications.

NaI (Tl) has the highest light output which allows a large number of crystal elements to be coupled to a single photo-detector. The light output refers more specifically to its efficiency for converting ionization energy to photons. The large light pulses are easily processed by conventional pulse-shaping electronics [27].

3.3.6 Comparison of a BGO to a NaI(Tl)

The comparison of NaI (Tl) (Z_I=53) to BGO (Z_B=74) shows that the probability for photoelectric absorption is about six times higher for BGO. BGO has three-times more stopping power for 511 keV photons than NaI (Tl), since the photoelectric interaction is more likely to occur with the higher atomic number. The likelihood of photoelectric interaction occurs if the energy of the incident photon is greater than the binding energy of the electron with which it interacts [23].

Equation 3.6 implies that the probability of photoelectric absorption (τ) is proportional to the cube of the atomic number of the interacting atom and inversely proportional to the cube of the energy.

$$\tau \propto \frac{Z^n}{(h\nu)^3} \tag{3.6}$$

where z is the atomic number of the detector material; and $h\nu$ is the energy of the absorbed photon.

If n varies between 3 and 4 over the γ-ray energy region of interest, the probability of photoelectric absorption increases rapidly with increasing atomic number of the absorber and decreases rapidly with increasing photon energy.

Equation 3.7 represents the photon absorption or scattering that leads to the exponential attenuation of the passage of photons through matter.

$$I = I_o e^{-\mu x} \tag{3.7}$$

where I is the total number of photons that have passed through a layer thickness x; I_o is the number of photons entering the material; μ is the linear attenuation coefficient of the material; and x is the thickness of the material [28].

The negative sign indicates that the number of γ-ray photons decrease as the beam penetrates the absorber.

If μ is equal to the probability per unit path that a γ-ray will have a collision in a medium, then $\lambda = 1/\mu$ is the mean free path of the γ-ray.

3.3.7 The PS-PMT used in Mineral-PET

Position Sensitive Photomultiplier Tubes (PS-PMTs) (Figure 3.7) consist of a photocathode sensitive to the scintillation light wavelength, multiple dynodes for photoelectron multiplication, and a pair of crossed multiple wire anodes. PS-PMTs have advantages over the regular PMT in that they can detect the relative position of occurrence of the incident photon. The scintillating material will preserve the position of the γ-ray because each pixel is optically isolated, and therefore the photons get channeled towards the surface of the detector. The incident photon hits the photocathode to produce the electrons. A paired anode array at the base of the PS-PMT records the electrons leaving the final dynode. The electronic chain is very similar to the previous discussion, incorpo-

Figure 3.7: The Position Sensitive Photomultiplier Tube

rating CFD for time peak-off, leading to a fast logic signal which can be used to build the event trigger logic and for time measurement. There are also spectroscopy amplifiers and ADCs, and in our case, a TDC (Time to Digital Converter) replaces the TAC. The CAMAC crate is replaced by a VME crate, which can handle a higher event rate and more complex control instructions.

3.3.8 The high-speed multi parameter event-by-event DAQ

The 64-channel high-speed multi parameter event-by-event Data Acquisition (DAQ) system (Figure 3.8) is a signal processing system. Each position sensitive detector has four channels. The 64-channel DAQ system is chosen because of the 16 detectors that will be placed on top and below the conveyor belt containing the kimberlite rocks. The DAQ must be used in order to identify the emission emanating from diamond carbon, using its high density compared to the kimberlite

background density. The DAQ is also used to gather the signals from the measurement sources and digitize the signals for storage, analysis and presentation in a computer.

There are several different modules which may be used in DAQ such as the Spectroscopy Amplifier, the CFD, the Gate and Delay component, the High Voltage Power supply, the computer module (VME), the ADC and the TDC.

The spectroscopy amplifier is used to amplify the electric pulses arriving from a pre-amplifier and processing them in such a way that they are suitable for the subsequent data analysing equipment. It is also used to shape the pulses (e.g. Gaussian).

The CFD is a signal-processing device, and is used to produce accurate timing information from analog signals.

The TDC is a device that converts the pulses into digital time indices, and can also be used to find important information about time of events.

The ADC is a device that converts an analog signal into a corresponding digital signal.

The electric pulses arriving at the anode of a PMT are very small and therefore require amplification to several volts before they can be further analyzed or processed. A pre-amplifier is always located as close to the PMT as possible because long connecting cables at this stage attenuate the signal significantly. The advantages of a pre-amplifier are to match the impedance of the detector to that of the electronics and to convert a charge pulse produced in the detector to a voltage pulse.

The High Voltage Power Supply must also be used in order to provide a stable voltage to the detector for optimum collection of charges [24].

Figure 3.8: The high-speed multi parameter event-by-event Data Acquisition System

3.3.9 The procedure used for constructing the position sensitive detector

The BGO crystal blocks of 10 mm thickness were coupled to the Hamamatsu Position Sensitive Photomultiplier Tubes (PS-PMTs). Transparent optical coupling grease was used between the PS-PMT and the crystal in order to minimize the internal reflection and wrapped with μ-metal foil for magnetic shielding. It was then seated in the light-tight jacket in order to minimize extra light and for mechanical protection. Plastic bolts were used to hold the PS-PMT stable. A measuring tape was used to measure the distance from the bottom of the BGO crystal to the PS-PMT for the exact measurement of the light-tight jacket [26].

There are different units of position sensitive detector i.e. the BGO crystal, the PS-PMT, the high voltage (HV) divider, and the anode read-out resistor chain circuit.

The anode read-out resistor chain circuit consists of four (X-, X+, Y-, Y+) position signal outputs, where the final signal can be taken. The outputs signal from each anode are divided through external resistive chains, and derived from X and Y electrodes as the position signal. The crossed wire anode construction is used for high spatial resolution, high position linearity, and easy signal processing for scintillation imaging. A mesh-dynode with excellent linearity and position sensitive crossed wire anode was used to enable the detection and the imaging of a wide variety of emission phenomena. An event-timing trigger was acquired in order to discriminate the energy signal from

the anode output.

Figure 3.9: Detector Construction

Chapter 4

Simulation of the single detector system and two detector system

4.1 Monte Carlo method

The Monte Carlo method is defined as representing the solution of the problem as a parameter of the hypothetical population, and using a random sequence of numbers to construct a sample of the population, from which the statistical estimates of the parameter can be obtained. A random number is a particular value taken on by a random variable [30]. A random variable is a variable that can take on more than one value, and for which any particular value that will be taken cannot be predicted in advance. Even though the value of the variable is unpredictable, the distribution of the variable may well be known. The distribution of a random variable gives the probability of a given value. If the solution of the problem is the result F, which may be a real number or a set of numbers, then the Monte Carlo estimate of F will be a function of the random numbers used in the calculations [31].

A random number is usually applied to a sequence of random numbers which, once they have been determined, are not at all random in the statistical sense but may have some properties which are similar to the properties of a truly random sequence. There are three different types of random sequences, namely truly random, pseudo-random and quasi-random. A perfect random sequence may have any distribution (Gaussian, uniform, etc) where a perfect uniform distributed sequence may not be at all random. A sequence of truly random numbers is unpredictable and therefore not reproducible. This sequence can only be generated by a random physical process (radioactive decay), thermal noise in electronic devices, and cosmic ray arrival time. The pseudo-random num-

bers are generated according to a strict mathematical formula and therefore reproducible and not at all random in the mathematical sense but are supposed to be indistinguishable from a sequence generated truly randomly [30]. Quasirandom numbers are numbers selected from a quasirandom sequence, which are useful in computational problems such as quasi-Monte Carlo integration. Quasi-Monte Carlo integration is a method of numerical integration that operates in the same way as Monte Carlo integration, but uses a sequence of quasirandom numbers to compute the integral [31].

The first large-scale calculations using the Monte Carlo method were studies of neutron scattering and absorption, random processes for which it is quite natural to employ random numbers. A subset of Monte Carlo calculation is known as direct simulation. The numerical results obtained were perfectly deterministic and obtainable by classical computational techniques (in fact, integration). The Monte Carlo method can be applied to a given problem and it does not depend on the stochastic nature of the system being studied, but only on the ability to formulate the problem in such a way that random numbers may be used to obtain the solution [31].

The Monte Carlo method may be applied wherever it is possible to establish equivalence between the desired result and the expected behavior of a stochastic system. The problem to be solved may be of a probabilistic or statistical nature, in which case its Monte Carlo formulation will usually be a straight forward simulation. The problem may be of a deterministic or analytic nature, in which case its Monte Carlo formulation may require some imagination and may appear artificial. All Monte Carlo calculations are equivalent to integrations, following the definition of a Monte Carlo calculation as producing a result F which is a function of a random number r_i [31].

Computer modeling by Monte Carlo methods was used in order to simulate the Mineral-PET system, since it is very good in solving coupled integral differential equations of radiation fields and energy transport, and is the leading method for studying radiation transport and interaction in materials. The method has been made practical by the fast memory access and computational speed of modern digital computers [32]. In Mineral-PET the Monte Carlo simulation was performed using the GEANT4 code.

4.1.1 The GEANT4 Simulation

GEANT4 is a toolkit used for Monte Carlo simulation of the passage of particles through matter. The toolkit is modular and flexible. The toolkit includes built-in steering routines and command interpreters which operate at the problem setup, run, event, particle transportation, visualisation, and analysis levels, allowing all parts of the toolkit to work in concert [34]. The toolkit is written in C++ and exploits advanced software-engineering techniques and object-oriented technology. The toolkit offers the user the ability to create a geometrical model with a large number of components of different shapes and materials, and to define elements that record information needed to simulate detector responses.

The capabilities of the toolkit include the materials involved, the generation of primary particle of events, the fundamental particles of interests, the generation of the event data, the storage of events and tracks, the response of sensitive detector components, the visualisation of the detector and particle trajectories, the geometry of the system, the physics processes governing particle interactions, the tracking of particles through materials, and the capture for subsequent analysis of simulation data at different levels of detail and refinement [34].

GEANT4 has been developed to provide the visualisation and the validation of the geometry inputs. The GEANT4 visualization system was developed in response to a diverse set of requirements such as quick response to study geometries and hits, tools to show volume overlap errors trajectories in detector geometries, and interactive picking to get more information on visualized objects. The simulation data, the detector components such as a piece of physical volume and logical volume, hits of particle in detector components, and the particle trajectories can be visualized [35].

The geometry is the analysis of the physical layout of the experiment, including the detectors, absorbers and how the layout will affect the path of the particle. A detector response is recorded when a particle passes through the volume of a detector and approximates how a real detector would respond. Run management records the details of each run, as well as setting up the experiments in different configurations between runs. The user interface is the aggregate of means by which the user interacts with the system. The user interface allows the user to manipulate a system and indicates the effects of the user manipulation [36].

There is a wide variety of user requirements on visualisation. The examples are, very quick response to survey successive events; high-quality outputs for presentation and documentation; im-

pressive special effects for demonstration; flexible camera control for debugging detector geometry and physics; selection of visualisable objects; interactive picking of graphical objects for attribute editing or feedback to the associated data; highlighting wrong intersections of physical volumes; and cooperative working with graphical user interfaces [34].

In Mineral PET, the data for the efficiency of the detection system was determined in order to validate the GEANT4 performed using the scint simulation, and to determine whether the coincidence measurement will reject all the non-511 keV photons.

4.1.2 Absorption length simulation

A simulation of the absorption length measurements is explained in Chapter 3. The main aim of this simulation was to determine the absorption length of γ photons in kimberlite and aluminum, in order to determine whether Monte Carlo simulation is efficient in calculating the absorption length of the 511 keV photons.

The numerical study using Monte Carlo was based on describing the geometry and the materials used and then tracking the photon's history from a source, through the sample to a detector.

The materials that were described in this simulation include the materials within the kimberlite, the elements of each material, the atomic number of each element, the atomic mass of each element, the density of each material, and the number of the element within each material. The absorption length must also be specified from the code in order to be determined by the geometry and the materials of the model.

The geometry and the materials of the model can also determine the absorption length of the materials, the absorption length of the scintillation detectors (e.g. BGO, NaI (Tl), BaF_2) and the absorption length of the ^{22}Na source.

A NaI (Tl) detector will generate a pulse that is proportional to the 511 keV energy deposited in the crystal by each event recorded. At the end of each count, the histogram that presents the counts recorded per increment of energy against energy was obtained.

The Gaussian fit was used to determine the absorption length of the kimberlite from the spectra.

The Gaussian fit provides the width of the peak and the error.

The analysis and the results of the absorption length simulation are presented in Chapter 5.

4.1.3 Tube reconstruction and the 3D tube density distribution simulation

The tube reconstruction and the 3D tube density distribution simulation are explained in Section 2.6. Computer modeling by the Monte Carlo method was used to determine whether the Mineral-PET detection system can identify the presence of possible diamond inclusion within the kimberlite rock. The relative position and the actual size of the possible diamond inclusion within the kimberlite can be reconstructed from the output of the Monte Carlo simulation of the systems.

A tube code is a simulation in which the number of events, the number of decays and hits, and the tubes were described in order to generate the background, and to generate background from the diamond, and also to generate the signal from the diamond. At the end of a certain number of events, a histogram that can be used to identify the size and the relative position of the inclusions was obtained.

The results of the tube reconstruction and 3D tube density distribution are presented in chapter 5.

4.1.4 Scintillation simulation

The main aim of scintillation (scint) simulation was to determine the efficiency of the detection system, by the coincidence of the two photons released upon the positron annihilation process. Since the coincidence condition is a very efficient filter in rejecting all non-diamond PET events or non-511 keV photons, then the coincidence detection was used in order to identify the presence of possible diamond inclusions within the kimberlite rock.

The apparatus used consisted of both position sensitive BGO detectors and a ^{22}Na source. A particle gun (^{22}Na) was placed between the two-position sensitive BGO detectors. The coincidence detection of two photons by the detectors on opposite sides of an object places the site of the annihilation on a line connecting the center of both detectors.

Scint simulation is a simulation in which the scintillation crystal, the rotational matrix of the crystal, the rotational angle of the crystal, the space between the crystals, the particle gun (radioactive

source), the thickness of the source, the position of the source, and the thickness of the absorber are described in the simulation.

The results of this simulation are presented in Chapter 5.

Chapter 5

Analysis, Results and Discussions

5.1 Absorption length measurements

5.1.1 Analytic determination of the absorption length

This section presents the analytical determination of the absorbtion length as explained in Chapter 3. A parameterised model can be used to determine the absorption length in cm of the aluminum from the theory which is 8.5 cm [24].

$$X_o = \left(\frac{716A}{Z(Z+1)ln(\frac{287}{\sqrt{Z}})} \right) \tag{5.1}$$

where 716 and 287 are parameters of the model; X_o is the absorption length; A is the atomic weight; and Z is the atomic number [37].

Substituting values for aluminum in the equation 5.1 gives X_o = 24.28 g.cm^{-2}, the absorption length needed to be scaled with density to be in the form of a distance that gives X_o = 8.9 cm.

To obtain an accurate value of the absorption length of the kimberlite using the parameterised model, the atomic number and the mass number of each element in the components were averaged. The expression of the absorption length in a mixture or compound was also used to determine the absorption length of the kimberlite from the theory using the chemical composite elements presented in Table 1.2.

The absorption length in a mixture or compound may be approximated by

$$\frac{1}{X_0} = \Sigma \frac{W_i}{X_i} \tag{5.2}$$

where w_i is the fraction by weight; and X_i is the absorption length for the ith element [37].

5.1.2 Experimental determination of the absorption length

This section presents the data for the absorption length determination as explained in Chapter 3. The computer analyzes the γ-ray data and uses the information to create a spectrum of the radiation absorbed. At the end of a certain number of events, a spectrum is recorded. The spectrum that represents the absorption of radiation depends on the material of the absorber, the γ-ray detection system, as well as the geometry of the detection system.

The following expression is used to determine the absorption length of the γ photons in the kimberlite and aluminum from the Monte Carlo simulation and the experiment.

$$I = I_o e^{-x/X_0} \tag{5.3}$$

where I is the number of photons with an absorber; I_0 is the number of photons without an absorber; X_0 is the linear attenuation coefficient of the material; and x is the distance.

Absorption length (in cm):

$$X_o = \left(\frac{L}{ln(\frac{I_0}{I})} \right)$$

where L is the length of the absorber.

Figure 5.1 illustrates the ^{60}Co source histogram taken with and without absorber from the DART system at the end of a certain number of events. The histogram presents the number of counts recorded per increment of energy against energy.

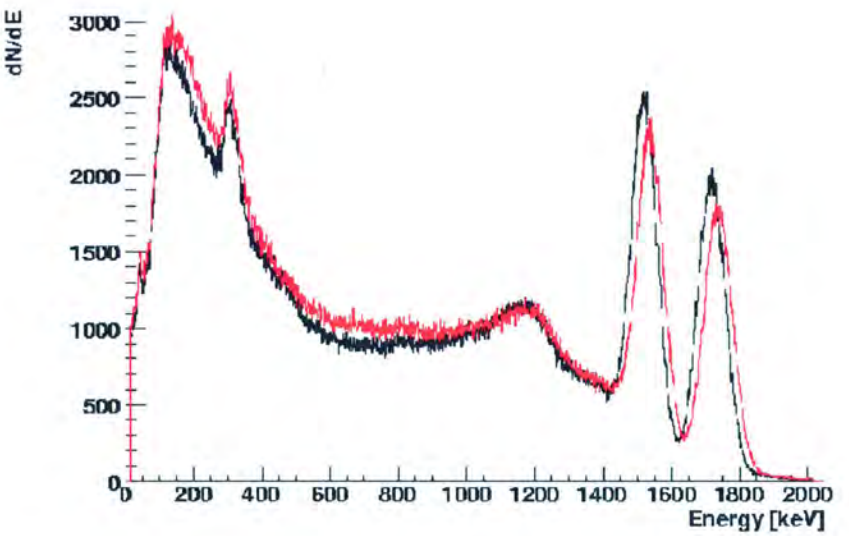

Figure 5.1: The comparison spectrum of the ^{60}Co source with and without the absorber from the DART system

The black spectrum is the spectrum of the ^{60}Co source placed 10 cm away from the NaI (Tl) detector (without absorber), and the red spectrum is the spectrum of a ^{60}Co source placed 10 cm away from the NaI (Tl) detector with absorber between.

The same real acquisition time was used in both the DART system and the Monte Carlo simulation. The fewer counts when the absorber is present enable the absorption length to be calculated.

I_o and I were extracted from the data by the Gaussian fit to the photo peak. ^{60}Co forms two peaks with energies of 1.173 MeV and 1.338 MeV. The 1.173 MeV peak was chosen in order to determine the absorption length of the kimberlite and aluminum.

A partial differential equation was used to derive the absorption length error expression from the absorption length expression. The purpose of the absorption length error is to estimate the accuracy of the results.

The following expression was used to determine the absorption length error:

$$\Delta X_o = |\frac{\delta X_o}{\delta I_o}|\Delta I_0 + |\frac{\delta X_o}{\delta I}|\Delta I \tag{5.4}$$

$$\Delta X_o = \left(\frac{L}{ln(\frac{I}{I_0})^2} \right)\left((\frac{\Delta I_0}{I_0}) + (\frac{\Delta I}{I}) \right) \tag{5.5}$$

where ΔI_0 is the square root of I_0; and ΔI is the square root of I.

5.1.3 Monte Carlo simulation determination of the absorption length

This section presents the data for the absorption length determination as explained in Chapter 3 and Chapter 4. In the Monte Carlo simulation, the kimberlite was modeled according to the material composition given in Table 1.2. This means that the atomic data was used in each element within each molecule for each contribution proportional to the weight % to simulate the composite material. This would then test the simulation of absorption length for a complicated composite.

Photons were released towards the absorber in a model of the set-up described in the previous section on the experimental determination of the absorption length. The Monte Carlo generated data were histogrammed and then analysed using the same algorithm as described above.

Figure 5.2 illustrates the histogram recorded at the end of a certain number of simulated events from the Monte Carlo simulation. The histogram presents the number of counts recorded per increment of energy against energy.

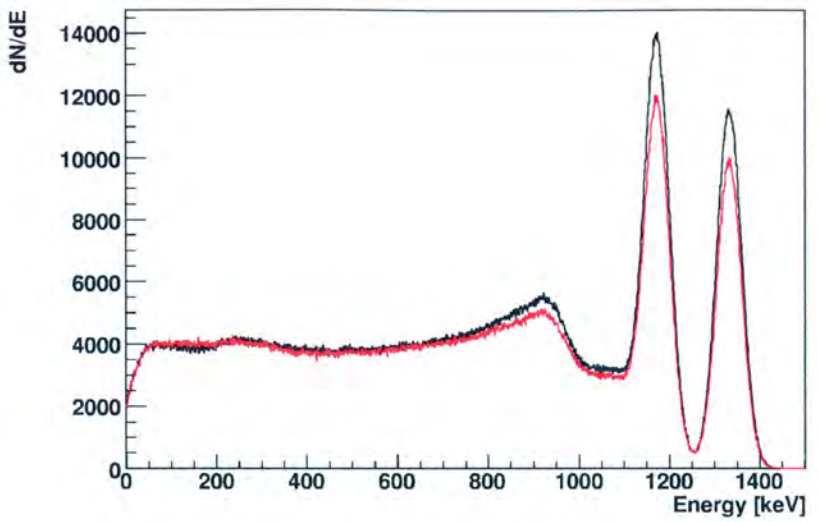

Figure 5.2: The comparison spectrum of the ^{60}Co source with and without the absorber from the Monte Carlo simulation

The black spectrum is the spectrum of the ^{60}Co source placed 10 cm away from the NaI (Tl) detector.
The red spectrum is the spectrum of a ^{60}Co source placed 10 cm away from the NaI (Tl) detector with absorber between.

5.1.4 The results of the absorption length measurements

The results of the absorption length as explained in Chapter 3 and Chapter 4 are summarised in Table 5.1.

Table 5.1 gives the absorption length of the aluminum and the kimberlite using Monte Carlo simulation, GEANT4, DART acquisition system (experiment) and theory.

Table 5.1: Absorption length Results

Peaks	Analytical (cm)	Geant4 (cm)	Monte Carlo (cm)	DART (cm)
Kimberlite	9.7	9.3	9.1 ± 0.21	8.9 ± 0.36
Aluminium	8.9	8.9	8.6 ± 0.18	8.5 ± 0.33

The difference in absorption length of aluminium ranges from 8.5 to 8.9 cm. The difference in absorption length of kimberlite ranges from 8.9 to 9.7 cm. The percentage error of the absorption length simulation is 2% and for experiment it is 4%

Since absorption length of the aluminum from the analytical formula is equal to the absorption length of the aluminum from the Geant material definition, therefore the results give a strong evidence that Geant4 is able to determine the absorption length of the kimberlite.

The absorption length of the kimberlite from the analysis of the Monte Carlo simulation is slightly different from the Geant4 material definition and the analysis of the experiment. Escaping of energy can cause the difference between these values. The first escape peak can be created if one of the 511 keV γ formed managed to escape the detector, the pulse generated will be 511 keV less than the original γ energy. Therefore to find the escape peaks, photo peaks must be identified over 1.022 MeV and (Eo-511) and (Eo-1.022) values must also be determined and a match to lower energy peaks must be monitored.

5.2 Timing measurement

5.2.1 Experimental determination of the timing measurement

This section presents the experimental determination of the time coincidence as explained in Chapter 3. The computer analyzes the γ-ray data and uses the information to create a spectra of the timing measurement. The timing spectrum depends on the positron annihilation, γ-ray detection system, and the geometry of the electronic system. The electronic configurations of timing measurements in Mineral-PET are designed to maximize the real coincidence events and minimize the random coincidences.

Figures 5.3 and 5.4 represent typical timing spectra showing the coincidence peaks recorded at the end of a certain number of events. These histograms present the number of counts against time in ps. The Range switch of the TAC was set at 0.1 and the multiplier switch at $\times 1$, the full-scale time range of which is 100 ns.

Figure 5.3 shows the linear spectrum of the timing coincidence obtained within the full-scale time range of 100 ns. This linear spectrum gives an excellent true coincidence, and indicates that due to

short resolving time the random coincidence events are very low. The full width at half maximum is low and the time resolution is very good.

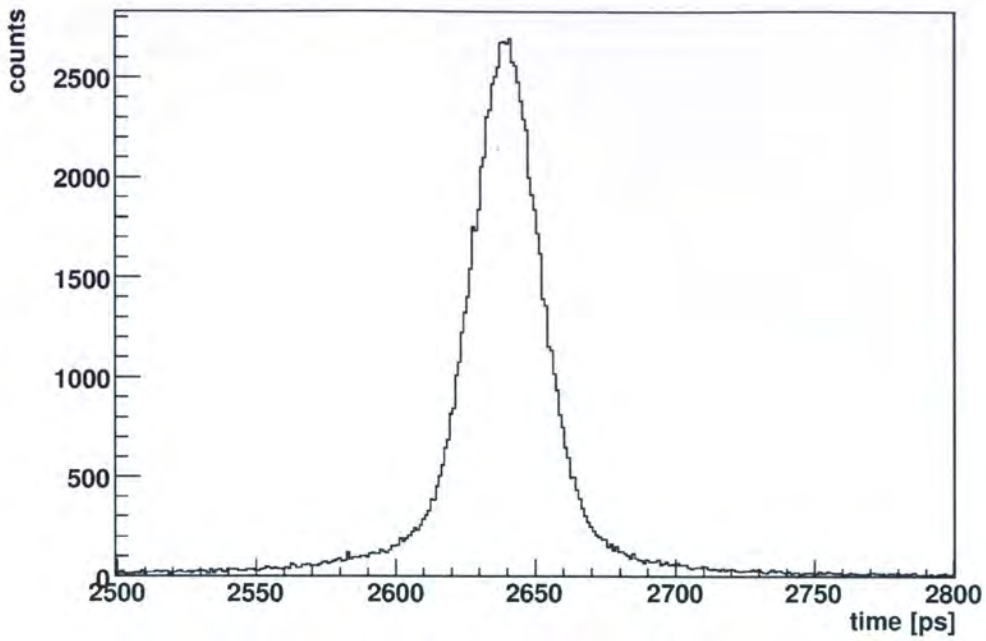

Figure 5.3: A typical timing spectrum showing the coincidence peak using BaF_2 detectors

The time resolution of the system was about 240 ps. The single count rate (SCR) in each detector was about 1500 Hz when the detectors were located close to the source, with SCR decreasing when the distance between the detector and the source increased. The total number of channels was 8192, where 1 ns was equivalent to 81.92 channels. The speed of light is 30 cm/ns. The log scale was used to obtain a better peak-shape and random rate of coincidence.

Figure 5.4 shows the spectrum of the timing coincidence obtained within the full-scale time range of 100 ns on a log scale. In this spectrum the top part is the Gaussian area and the middle to bottom part is the Lorentzian area while the tail part is due to background. The data was analyzed using the Gaussian expression and the Lorentzian expression, but due to the short time the random coincidences could not be evaluated. The log scale was used to characterise the peak shape. Even though the peak shape could be characterised, it was not possible to determine the random coincidence.

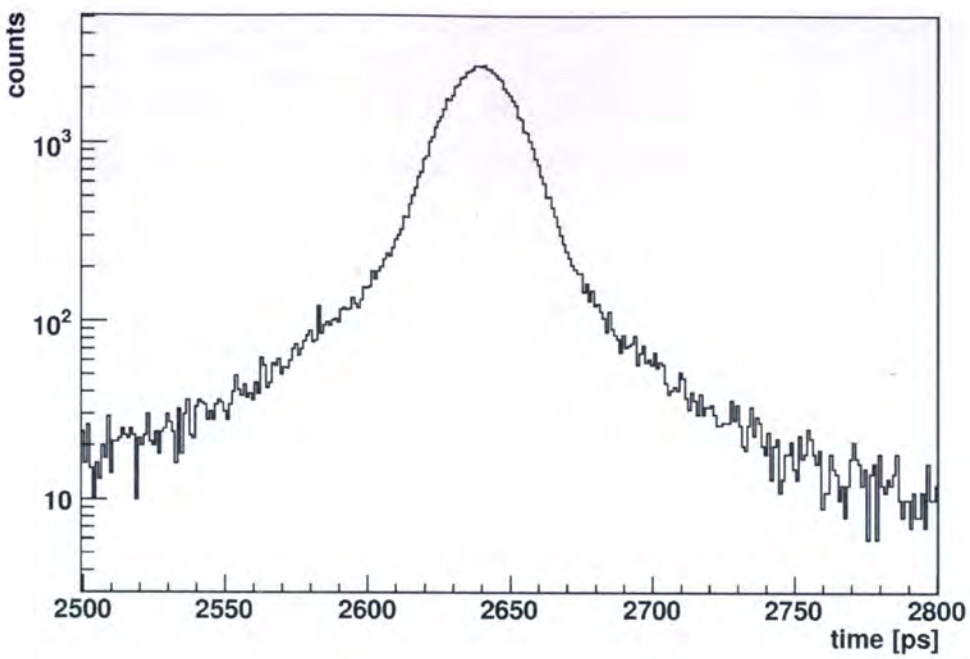

Figure 5.4: A typical timing spectrum showing the coincidence peak as obtained within the full-scale time range of 100 ns using BaF_2 detectors with a short range

The following expressions were used to determine the Gaussian area and the Lorentzian area in order to calculate the area of real coincidence.

Equation 5.2 presents the Gaussian distribution:

$$G(x) = \frac{p_0}{\sqrt{2\pi}} e^{-\frac{(x-p_2)^2}{2p_1^2}} \tag{5.6}$$

Where p_0 is the area; p_2 is the mean/centre; and p_1 is the variance.

Therefore the Gaussian function is presented as

$$A_G = \frac{p_0}{\sqrt{2\pi}} p_1$$

.

Equation 5.3 presents the Lorentzian distribution:

$$L(x) = \frac{p_1 p_2}{2\pi} \frac{\mathrm{d}x}{(x - p_0)^2 + 0.25 p_2^2} \tag{5.7}$$

where p_0 is the center; and p_2 is the parameter specifying the width.

The Lorentzian function is presented as;

$$A_L = p_1$$

The area of real coincidence is given by equation 5.4

$$A_{real} = A_G + A_L \tag{5.8}$$

5.2.2 The results of time coincidence measurements

This section presents the results of the time coincidence explained in Chapter 3. The random was evaluated using the Lorentzian, Gaussian and exponential functions (Figure 5.5) as explained in Section 5.2.1.

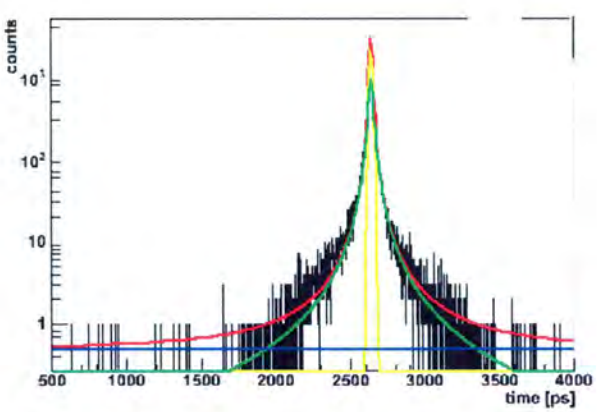

Figure 5.5: A coincidence curve of the timing measurements

The black spectrum indicates the time coincidence spectrum, the yellow line indicates the Gaussian, the green line indicates the lorentzian, and the blue line indicates the background.

Using a ^{22}Na, the coincidence spectrum will result in a suppressed 1274 keV peak and Compton continuum. The 511 keV photons will travel in opposite directions from the source along the same line, while the 1274 keV photon has an isotropic direction relative to the annihilation photon. Thus, the 1274 keV peak is expected to be suppressed in the coincidence spectrum since only a fraction, determined by the solid angle subtended by the detector, will interact in the detector. Some chance coincidence background may also be present.

The source was located between the two detectors, thus one would expect the 511 keV peak to have the same area in both energy and coincidence spectra if the opposite detector have a 100% detection efficiency.

Figure 5.6 shows the spectrum of the timing coincidence obtained within the full-scale time range of 100 ns on a log scale with a long range. It is now clearer that a low level rate of random coincidences were obtained. The random rate was analysed even further to ensure that its details were correctly understood and conformed to the expectations of the theory (Section 3.2.2).

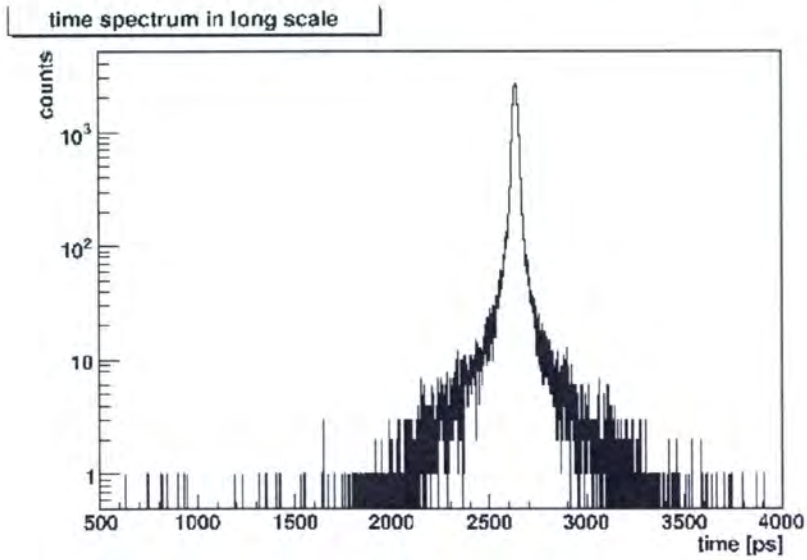

Figure 5.6: A typical timing spectra showing the coincidence peak as obtained within the full-scale time range of 100 ns using BaF_2 detectors with a long range

5.2.3 Experimental determination for the study of the random rate

This section presents the random rate data explained in Chapter3. The rate of random coincidence (N_r) on a short time scale is very low and therefore difficult to quantify. Therefore, in order to obtain the random coincidence, the detectors were placed 90^0 to each other with a time range increasing from 100 ns to 80 μs.

Figure 5.7 presents a typical spectrum of the random rate at the end of a certain number of events.

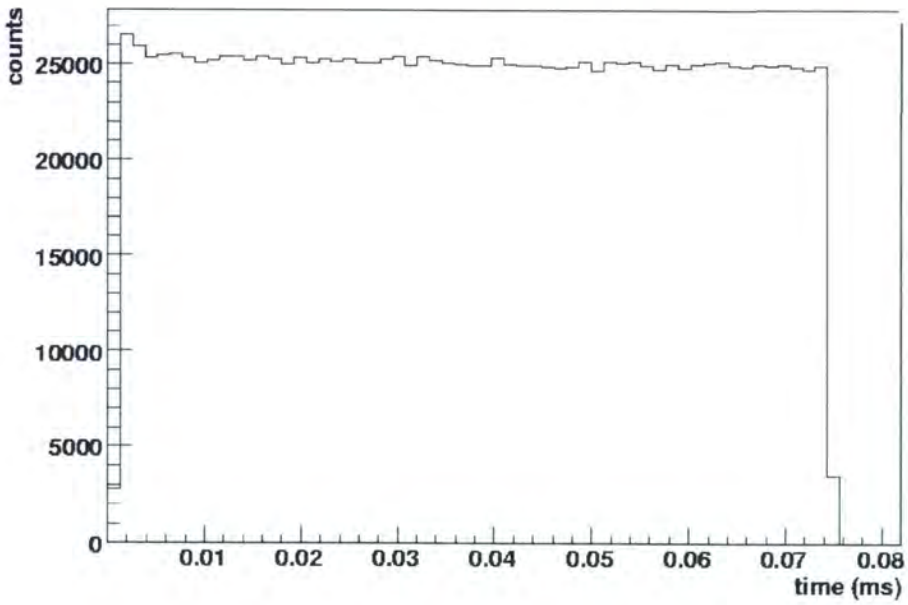

Figure 5.7: A typical timing spectra showing the random coincidence peak as obtained using BaF_2 detectors

5.2.4 The results obtained from the study of the random rate

Figure 5.8 presents the exponential curve of the random coincidence as determined in Equation 3.5, where the single rate can be extracted.

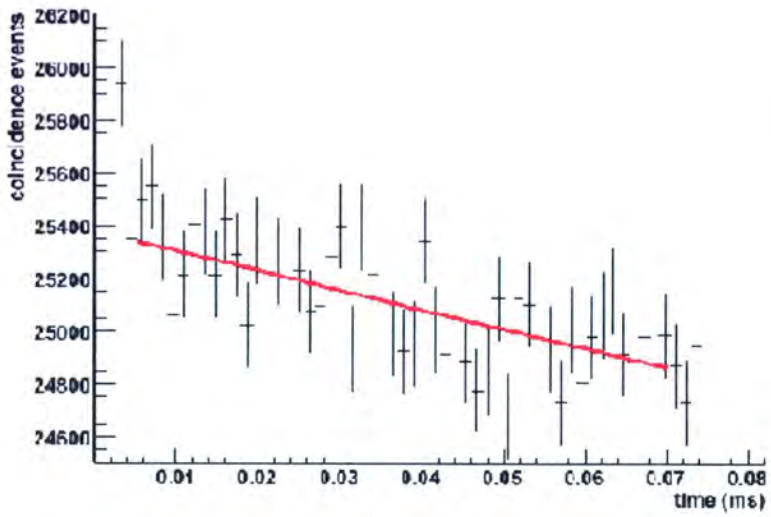

Figure 5.8: A random curve of the BaF_2 detectors

5.3 Results obtained from tube reconstruction and the 3D tube density distribution simulation

Figure 5.9 presents the results of the tube simulation explained in Section 2.6 and Chapter 4. The main purpose of this simulation was to prove whether the Mineral-PET algorithm is efficient to determine the relative position and the actual size of the possible diamond inclusion within the kimberlite.

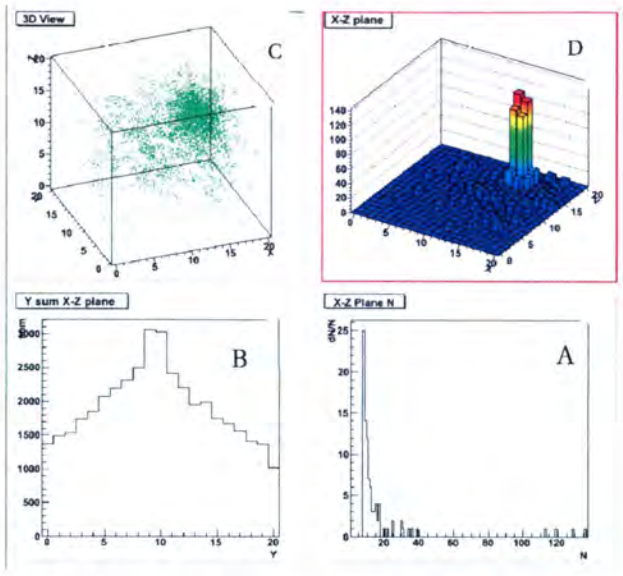

Figure 5.9: Tube reconstruction and 3D tube density distribution

Figure A in Figure 5.9 presents the histogram obtained at the end of certain events from the simulation. The histogram presents the number of counts recorded per increment of energy against energy. The position of the inclusions is not clear, therefore a range can be set in order to indicate the position of the inclusions within the kimberlite (Figure B).

Figure C in Figure 5.9 indicates some inclusions within the kimberlite. Since the non-diamond carbon is assumed to be homogeneously distributed in kimberlite, whereas the Mineral-PET algorithm is looking for a significant hot spot of localised carbon, an energy window must be set in order to eliminate the noise arising and to select only the 511 keV photons.

Figure D in Figure 5.9 presents a histogram visualised at the plane intersecting the position of the one carat diamond.

Figure C and Figure D in Figure 5.9 indicate that the false intersections have a systematic distribution and contribute to a signal indicating the presence of a diamond. The false intersections effectively amplify the recognition signal and increase the statistical significance of the results. Figure D indicates the higher probability of noise in the vicinity of the diamond. The results indicate an excellent signal to noise ratio.

5.4 Results from Monte Carlo (scint) simulation

This section presents the results for the Monte Carlo (scint) simulation explained in Chapter 4. GEANT4 simulation of a two detection system was used to simulate the efficiency of the detection system by the coincidence of the two 511 keV photons released upon the positron annihilation process. Scint simulation provides a visualisation of coincidence detection that can be used to identify the presence of possible diamond inclusions within kimberlite (Figure 5.10). These results gave strong evidence that scint simulation is able to reject all non-diamond positron emitter events or non-511 keV photons.

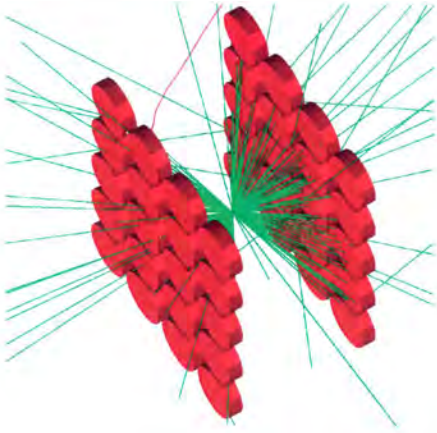

Figure 5.10: Annihilation Coincidence Detection

Chapter 6

Conclusions

The main aim of this system is to detect the possible diamond inclusion in the kimberlite rock, and not only their presence but also their size and their relative position. Several measurements were performed to ensure the feasibility of the system. The study of the absorption length of the γ-ray attenuation in kimberlite material was determined using the DART acquisition system (experimentally), analytical expression (theoretically), and with the aid of computer model using the Monte Carlo simulation (theoretically). The results obtained from both simulation and measurements were similar to each other. A good agreement between simulation and data analyses indicates that GEANT4 is capable of describing the Mineral PET.

The study of the ability of the coincidence condition in the detection system to reduce noise in the context of high count rate of both PET and non-PET isotopes was also performed. The main purpose of the timing measurement was to extract the random coincidence rate from the real coincidence rate. The study proved that the random coincidence can be effectively extracted from the real coincidence using a short resolving time. The timing measurement validated the model for evaluating the effects of the random co-incidence rate and gave strong evidence that the Mineral-PET algorithm is able to discriminate very well between random coincidences and real coincidences.

Therefore, the absorption length measurements and the timing coincidence measurements have proved the feasibility of the Mineral PET system and the efficiency of the detection system.

Chapter 7

Appendices

7.1 Appendix A

7.1.1 The experimental determination of the time calibration measurement for the time coincidence measurement

This section presents the data for the time calibration determination as explained in Section 3.2.4. The time calibration spectrum is acquired using a module that generates a sequence of start and stop pulses with different time delays called a time calibrator. Figure 7.1 presents a typical spectrum showing the time calibration at the end of a certain number of events. This measurement was based on the time measurement where the range switch of the Time to Amplitude Converter (TAC) was set at 0.1 and the Multiplier switch at $\times 1$, with the full-scale time range of 100 ns. The delay period of the time calibrator was set at 0.01 μs for the time interval between start and stop pulses. The range of the time calibrator was set at 0.16 μs. The rate of the time calibrator was set at 3.2 kHz.

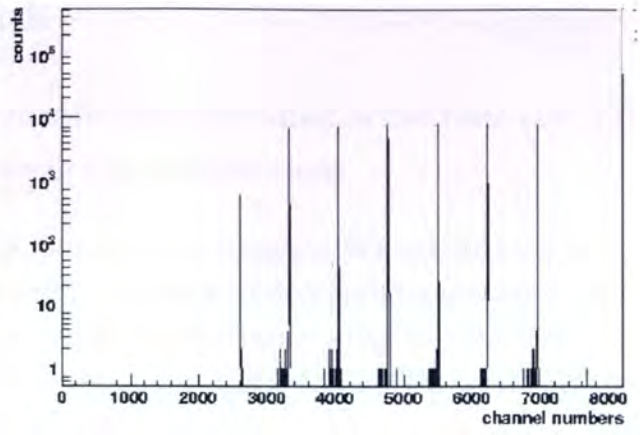

Figure 7.1: Time calibration for the timing measurements

7.1.2 The results of time calibration measurements for time coincidence measurement

The results presented in Figure 7.2 give the time calibration plot with TAC of a full-scale time range of 100 ns.

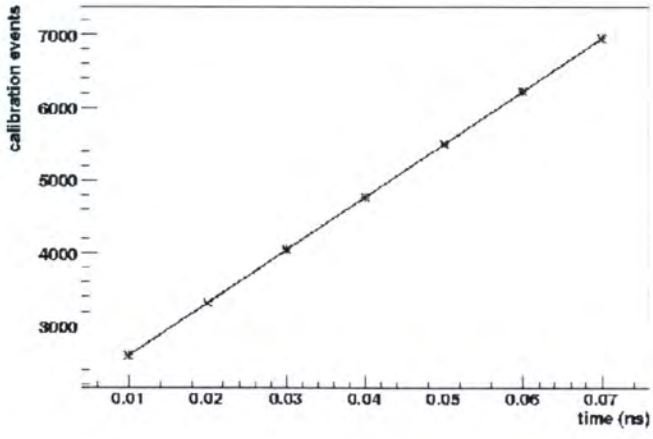

Figure 7.2: Time calibration for the timing measurements

where in terms of section 5.2.1, Po = $1.186e^{3\pm2.717}$; and P1 = $7.262e^{4\pm60.521}$

7.2 Appendix B

7.2.1 The experimental determination of the time calibration measurement for the study of the random rates

Figure 7.3 shows a typical spectrum showing the time calibration at the end of a certain number of events. This measurement was based on the time measurement where the range switch of the TAC was set at 0.8 μs at the Multiplier switch at ×100, of which the full-scale time range was 80 μs. The period of the time calibrator was set at 5.12 μs. The range of the time calibrator was set at 81.92 μs. The rate of the time calibrator was set at 4 kHz.

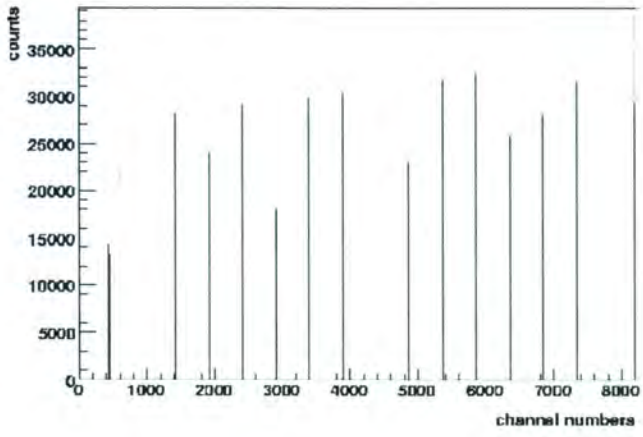

Figure 7.3: Time calibration for the study of the random measurements

7.2.2 The results of the time calibration measurements for the study of the random rate

The results presented in Figure 7.4 give the time calibration plot with a TAC full-scale time range of 80 μs.

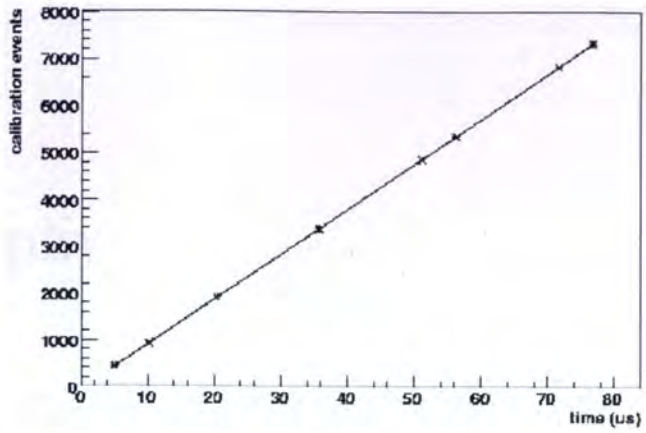

Figure 7.4: Time calibration for the study of the random rate

where in terms of section 5.2.1, Po = $-5.419e^{1\pm0.2371}$; and P1 = $9.623e^{1\pm0.004627}$
Figure 7.2 and figure 7.4 show that the time measurements are properly calibrated.

7.3 Appendix C

7.3.1 The data obtained from energy measurement

This section presents the data for the energy measurements explained in Chapter 3. Figure 7.5 shows a typical energy spectrum showing the energy peak at the end of a certain number of events.

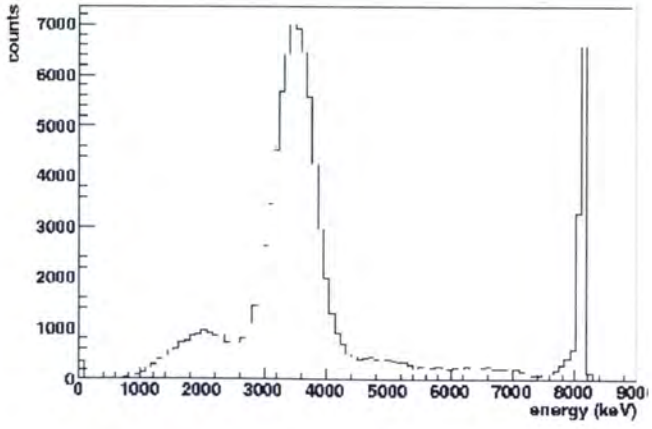

Figure 7.5: A typical energy spectrum showing the energy peak as obtained using BaF_2 detector

Bibliography

[1] Connell et al. 2004. Feasibility study of Mineral PET. (Feasibility study delivered as part of the research) (Unpublished)

[2] Sellschop, J and Connell, S. 2005. Detection of diamonds. *http://www.patents/.*

[3] Sinha, A. 2007. Advanced in x-ray and neutron imaging and its application. *http://www.barc.gov.in/publication/200710-3.pdf.*

[4] Carts-Powell, Y. 2002. Electronic Imaging and Signal Processing. *http://www.spie.org.*

[5] Langner, J. 2003. Development of a parallel computing optimized head movement correction method in positron emission tomography. *http://www.jens-langer.de/ftp/MScThesis.pdf.*

[6] Committes from American College of Radiology. 2008. Positron emission tomography scanning. *http://en.wikipedia.org/wiki/Positron emission tomography.*

[7] University of Virginia. 2007. Positron emission tomography. *http://www.healthsystem.virginia.edu/UVAHealth/adult. radiology/pet.cfm.*

[8] Annenkov, A., Borissevitch, A., Dossovitski, A., Missevitch, O., Korzhit, M., Federovand, A. and Lecoq, A. 2006. Development of scintillation material for pet scanners. *Institute for Nuclear problems, Bogoroditsk Techno Chemical Plant, JSC NeoChem and CERN.*

[9] Herzog, H, 2007. Methods and applications of positron-based medical imaging. (Radiation Physics and Chemisty 76 (2007) 337-342).

[10] Wolf-Dieter, H. and Phelps, M.E., 1983. Positron Emission Tomography Of The Brain. (Springer-Verlag).

[11] Heston, C. 2000. Imaging for hope. *The academy of Molecular Imaging.*

[12] Melcher, C.L. 2007. "Scintillation crystal for positron emission tomography". *The Journal of Nuclear Medicine.* (Vol 41. No6).

[13] Ramsey B. 1999. Introduction to pet physics: The physical principles of pet.

[14] Ollinger, J.M. and Fessler, J.A. 2006. Positron emission tomography. *IEEE Signal Processing Magazine* 14(1):43-45, Jan 1997.

[15] David Rollo, F., Everette James, A., Coulom, C.M., and Ericson, J.J. 1981. The physical basis of Medical Imaging. *Appleton-centuary-crafts, New York.*

[16] The Atlas of Canada. 2004. Location of kimberlites. *http://atlas.nrcan.gc.ca/site/english/maps/economic/diamondexploration/loca.*

[17] Pell, J. 2007. Kimberlite-hosted diamonds. *British Columbia Geological Survey.*

[18] Gadioli, E., Hodgson, P.E and Gadioli Erda, E. 1997. Introduction to Nuclear Physics. *Clarendon Press.*

[19] Schelbert, H.R., Phelps, M.E. and Mozziotta, J.C. 1986. Principles and Applications for the Brain and Heart. *Raven Press Book, Ltd.*

[20] Price, W.J. 1992. Nuclear Radiation Detection. *McGraw-Hill, Inc*, 2nd ed.

[21] European Space Components Information Exchange System Organization (escies.org). 2006. Cobalt. *European Space Components Information Exchange System Organization.*

[22] Huber, A.C. and Pantazis, J.A. 2007. Gamma ray detection system. *Amptek Company.*

[23] Knoll, G.F. 2000. *Radiation detection and measurement, third edition.* John Wiley and Sons,Inc.

[24] Leo, W.R. 1993. *Techniques for Nuclear and Particle Physics Experiments.* Spriger-Verlag: New York.

[25] Burgham, W.E. 1963. *Introduction to Nuclear Physics.* Longman Group Limited.

[26] Sorenson, J.A. and Phelps, M.E. 1987. *Physics in Nuclear Medicine 2nd edition.* W.B Sounders Company.

[27] Knoll G.F. 1997. *Radiation detection and measurement.* John Wiley and Sons,Inc.

[28] Hendee, W.R. 1970. *Medical Radiation Physics.* Year Book Medical publisher, Inc.

[29] Early, P.J. Rozzak, M.A. and Sodee, B.D. 1985. *Nuclear Medicine Technology 3rd edition.* C.V Mosby Company, S.T Louis.Toronto. Princeton.

[30] James, F. 1980. Monte carlo theory and practice. *Experimental Techniques in High Energy Physics, Vol.43 (1980) 627-659.*

[31] Ferbel, T. 1994. *Experimental Techniques in High Energy Physics.* Wesley Publishing Company,Inc.

[32] Lab TA Joy Woller. 1996. The basics of monte carlo simulations. *University of Nebraska-Lincoln, Physical Chemistry Lab (Chem 484).*

[33] Hammersley, J.M. and Handscomb, D.C. 1964. *Monte Carlo Methods.* John Wiley and Sons,Inc.

[34] Agostinelli, S. 2003. Geant4 - a simulation toolkit. *Nuclear Instruments and Methods in Physics Research A 506 (2003).*

[35] GEANT4 User Support. 2007. Geant4 user's guide for toolkit developers. *GEANT4 Collaboration.*

[36] Allison et al. 2006. Geant4 development and applications. *IEEE Transactions on Nuclear Science, Vol.53, No.1.*

[37] Groom, D.E. Bichsel, H. and Klein, S.R. Jan 1 (2006). Passage of radiation through matter. *Journal of Physics G33.*

[38] Chandra, R. 1992. *Introductory Physics of Nuclear Medicine, fourth edition.* lea and Febiger, Philadelphia.

[39] Early, P.J. and Sodee, D.B. 1985. *Principles and Practice of Nuclear Medicine.* C.V Mosby Company, 1985.